

Switching state to engage and sustain attention: Dynamic synchronization of the frontoparietal network

Grace Ross^{a,b,c}, Wei A. Huang^{a,b,c}, Jared Reiling^d, Mengsen Zhang^d, Jimin Park^{a,b}, Susanne Radtke-Schuller^{a,b}, Joseph Hopfinger^a, Agnieszka Zuberer^{a,b}, Flavio Frohlich^{a,b,c,e,f,g,*}

^a Department of Psychiatry, University of North Carolina at Chapel Hill, Chapel Hill, NC, USA

^b Carolina Center for Neurostimulation, University of North Carolina at Chapel Hill, Chapel Hill, NC, USA

^c Neuroscience Center, University of North Carolina, Chapel Hill, NC, USA

^d Department of Computational Mathematics, Science, and Engineering, Michigan State University, East Lansing, MI, USA

^e Department of Cell Biology and Physiology, University of North Carolina, Chapel Hill, NC, USA

^f Department of Biomedical Engineering, University of North Carolina, Chapel Hill, NC, USA

^g Department of Neurology, University of North Carolina, Chapel Hill, NC, USA

ARTICLE INFO

Keywords:

Sustained attention
Frontoparietal network
Rhythmic synchronization
Cortical oscillations

ABSTRACT

Sustained attention (SA) is essential for maintaining focus over time, with disruptions linked to various neurological and psychiatric disorders. The oscillatory dynamics and functional connectivity in the dorsal frontoparietal network (dFPN) are crucial in SA. However, the neuronal mechanisms that control the level of SA, especially in response to heightened attentional demands, remain poorly understood. To examine the role of rhythmic synchronization in the dFPN in SA, we recorded local field potential and single unit activity in ferrets that performed the 5-Choice Serial Reaction Time Task (5-CSRTT) under both low and high attentional load. Under high attentional load, dFPN exhibited a pronounced state shift that corresponded with behavioral changes in the animal. Prior to the onset of the target stimulus, animals transitioned from a stationary state, characterized by frontal theta oscillations and dFPN theta connectivity, to an active exploration state associated with sensory processing. This shift was indexed by a suppression of inhibitory alpha oscillations and an increase in excitatory theta and gamma oscillations in parietal cortex. We further show that dFPN theta connectivity predicts performance fluctuations under high attentional load. Together, these results suggest that behavioral strategies for maintaining SA are tightly linked to neuronal state dynamics in the dFPN. Importantly, these findings identify rhythmic synchronization within the FPN as a potential neural target for novel therapeutic strategies for disrupted attention.

1. Introduction

Sustained attention (SA) describes the capacity to remain vigilant and respond to unpredictable and behaviorally relevant stimuli over time. Impairments in this process are transdiagnostic and associated with attention deficits and impulsivity (Barkley, 1997; Bora et al., 2006; Goswami et al., 2009; Nuechterlein et al., 2015; Pagliaccio et al., 2017; Tucha et al., 2017). The dorsal frontoparietal network (dFPN) plays a crucial role in supporting SA. For example, fluctuations in low frequency activity (0.01–0.08 Hz) within the dFPN were detected in human fMRI data and negatively correlated with accuracy in a psychomotor vigilance

task performed after sleep deprivation, a condition known to impair SA (Yao et al., 2023; Durmer and Dinges, 2005; Drummond et al., 2005). Activity within the dFPN is also influenced by task performance (Weissman et al., 2006). Specifically, fMRI results during a selective attention task show a reduction in activity in frontal cortical areas immediately before an attentional lapse, followed by increased activity afterward, potentially reflecting a refocusing of attention. Collectively, these findings highlight the dynamic role of the dFPN in regulating and maintaining attentive behavior.

Dynamic regulation of attention is imperative, as attention fluctuates on a moment-to-moment basis during sustained task engagement

* Corresponding author at: Department of Psychiatry, University of North Carolina at Chapel Hill, Chapel Hill, NC, USA.

E-mail address: flavio_frohlich@med.unc.edu (F. Frohlich).

(Esterman et al., 2013; dedeBettencourt et al., 2015; Rosenberg et al., 2016). These fluctuations are closely tied to cortical oscillations, which provide insight into how attention is rhythmically sampled by reflecting changes in neuronal excitability (Helfrich et al., 2018). In particular, oscillatory activity within the dFPN has been shown to support attentional control, in both human (Clayton et al., 2015; Helfrich et al., 2018) and animal studies of SA (Sellers et al., 2016; Huang et al., 2024). According to an oscillatory model of SA, frontal theta oscillations play a crucial role in monitoring the need for cognitive control and activating relevant processes. Meanwhile, alpha oscillations inhibit allocation of attentional resources to irrelevant stimuli, and gamma oscillations enhance task-relevant network activity (Clayton et al., 2015).

Frontal theta oscillations, especially, have been extensively studied in relation to cognitive control (Cavanagh and Frank, 2014). Recent research has highlighted the causal role of frontal theta power in cognitive effort (McFerren et al., 2021) and prioritization of task relevant information (Riddle et al., 2020; 2024) in working memory (WM) tasks. During a 5-choice continuous performance task designed to measure SA, increased response-locked theta power was observed in human participants under more challenging task conditions (Cavanagh et al., 2021). However, enhancing frontal theta oscillations is a finite cognitive resource and excessive mental effort can deplete these resources (Yu et al., 2022), leading to diminished attentional capacity (Nielsen et al., 2001). Suggesting that cognitive exhaustion may be a key factor in attentional disruption.

Theta oscillations also play a key role in orchestrating inter-areal communication during cognitive tasks, including working memory (Johnson et al., 2023) and SA (Sellers et al., 2016; Marek and Dos-enbach, 2018). This communication is facilitated via phase synchrony which enables flexible information encoding during behavior. A recent study demonstrated the causal role of frontoparietal theta connectivity in information prioritization and parietal alpha oscillations in suppression of task-irrelevant information, during a WM task with targeted TMS (Riddle et al., 2024). Additionally, in an animal model, enhancement of frequency specific network connectivity within the posterior visual network (LP/Pulvinar, posterior parietal cortex and visual cortex) was shown to improve performance during a preclinical SA task (Huang et al., 2024). Specifically, rhythmic optogenetic perturbation at theta frequency in the LP/Pulvinar increased cortico-thalamic spike-field coherence, which was correlated with improved task accuracy. These findings underscore the importance of frequency-specific network connectivity in supporting behavior during cognitive tasks. However, despite our understanding of how the dFPN is functionally connected via theta phase synchrony during SA (Sellers et al., 2016), it remains unclear how this connectivity flexibly adapts to varying levels of attentional demand.

In the present study, we examine how oscillatory dynamics of the dFPN differ between periods of low and high attentional demand and how these differences relate to behavioral performance. To increase the demand for attentional resources, we modified an established preclinical SA task, the 5-Choice Serial Reaction Time Task (5-CSRTT). The 5-CSRTT is a preclinical analog to the continuous performance task previously used to evaluate attentional deficits in humans (Carli et al., 1983; Fang and Frohlich, 2023). In brief, the 5-CSRTT is a self-paced, freely moving visual attention task in which an animal must initiate a trial and wait for a variable delay to respond to a visual stimulus and retrieve water reward. Notably, while the original human CPT included non-target trials to directly assess impulse control, the 5-CSRTT does not. Rather, in the 5-CSRTT, we take a holistic approach and examine top-down inhibitory control in the context of task engagement. Importantly, SA is unique from other domains of attention in that it specifically refers to the ability to maintain engagement with a single task or stimulus over time without lapsing (Sarter et al., 2001). In the context of the 5-CSRTT, SA is required during the delay period when animals must remain engaged with the stimulus screens (Sellers et al., 2016; Fang and Frohlich, 2023; Huang et al., 2024).

This trial-based measurement of SA differs from human literature, where SA is commonly assessed throughout a session (Esterman and Rothlein, 2019) using two cardinal measurements: moment-to-moment fluctuations in attention captured by response latency variability, and vigilance decrements over time reflecting general fatigue. Rather than increasing demand on attention through fatigue effects, we aimed to isolate correct trials where animals engage the neural networks required for SA under more attentionally demanding conditions. Therefore, we manipulated attentional load by lengthening the 5-CSRTT delay period, increasing the demand for attentional resources by requiring engagement for a longer period of time.

To identify the neural dynamics of the dFPN during periods of higher attentional demand and lower behavioral performance, we simultaneously recorded electrophysiology from the two nodes of the ferret dFPN during the 5-CSRTT. This study was conducted in ferrets because they are an advantageous model for studying the frontal cortex (Ross et al., 2024), have task modulated posterior alpha oscillations (Stitt et al., 2018; Huang et al., 2024) and a functionally connected dFPN (Sellers et al., 2016). We then analyzed and compared local field potential, network functional connectivity and single unit dynamics when attentional load was low versus when load was high, and related our neural findings to animal behavior. We found that a longer 5-CSRTT delay period significantly degraded task performance and induced a shift in dFPN oscillatory dynamics that aligned temporally with distinct behavioral states. Our results further demonstrate a relationship between dFPN theta connectivity and attentional performance in the 5-CSRTT. In summary, we demonstrate how increased demand on attentional resources modulates dFPN oscillatory dynamics and contributes to SA.

2. Results

2.1. Novel 5-CSRTT manipulation increases attentional load, degrades task performance

We hypothesized that a longer delay would induce higher attentional load as compared to the shorter delay, due to the prolonged cognitive effort required to avoid distractions and maintain vigilance. To prevent animals from becoming habitual in their task performance, we included a small subset of other delay lengths in each task condition (Fig. 1aii), but analyzed only the principal delay lengths (4 s short-delay, 9 s long-delay). Our results demonstrate that behavioral performance was significantly degraded when the delay was long compared to when it was short (Fig. 1c&d). Overall accuracy (% correct/total trials) was reduced during long-delay sessions (mean: short 74 % vs long 63 %, $p = 0.03$; Fig. 1d), primarily driven by an increased occurrence of premature (mean: short 1 % vs long 17 %, $p < 0.001$) and incorrect touches (mean: short 5 % vs long 14 %, $p < 0.001$; Fig. 1d). Post-stimulus accuracy (see Methods) was not significantly different between task conditions (mean: short 74 % vs long 75 %, $p = 0.43$; Fig. 1d), indicating that performance decreased in the long-delay task likely due to weakened inhibitory control rather than impaired detection accuracy. In the short-delay sessions, the most common non-correct response was an omission (mean: short 20 % vs long 5 %, $p < 0.001$). Additionally, in long-delay trials, animals responded to the visual stimuli faster (mean: short 1.56 s vs long 0.89 s, $p < 0.001$) and retrieved water rewards after correct trials more slowly (mean: short 1.37 s vs long 1.53 s, $p < 0.001$) (Fig. 1c). We also analyzed how accuracy changed within a session by calculating accuracy in a sliding window (5 trials) and extracting the slope and corresponding p-value from linear regression, within each session type per animal. We found that overall, accuracy increased over the course of a session in both the long-delay (Animal A: 0.087 ± 0.54 , $p = 0.23$, Animal B: 0.36 ± 0.34 , $p = 0.27$, Animal C: 0.38 ± 0.35 , $p = 0.17$) and short-delay (Animal A: 0.37 ± 0.51 , $p = 0.05$, Animal B: 0.36 ± 0.19 , $p = 0.05$, Animal C: 0.22 ± 0.11 , $p = 0.29$) condition with marginal significance, suggesting there is not a time-on-task effect. We

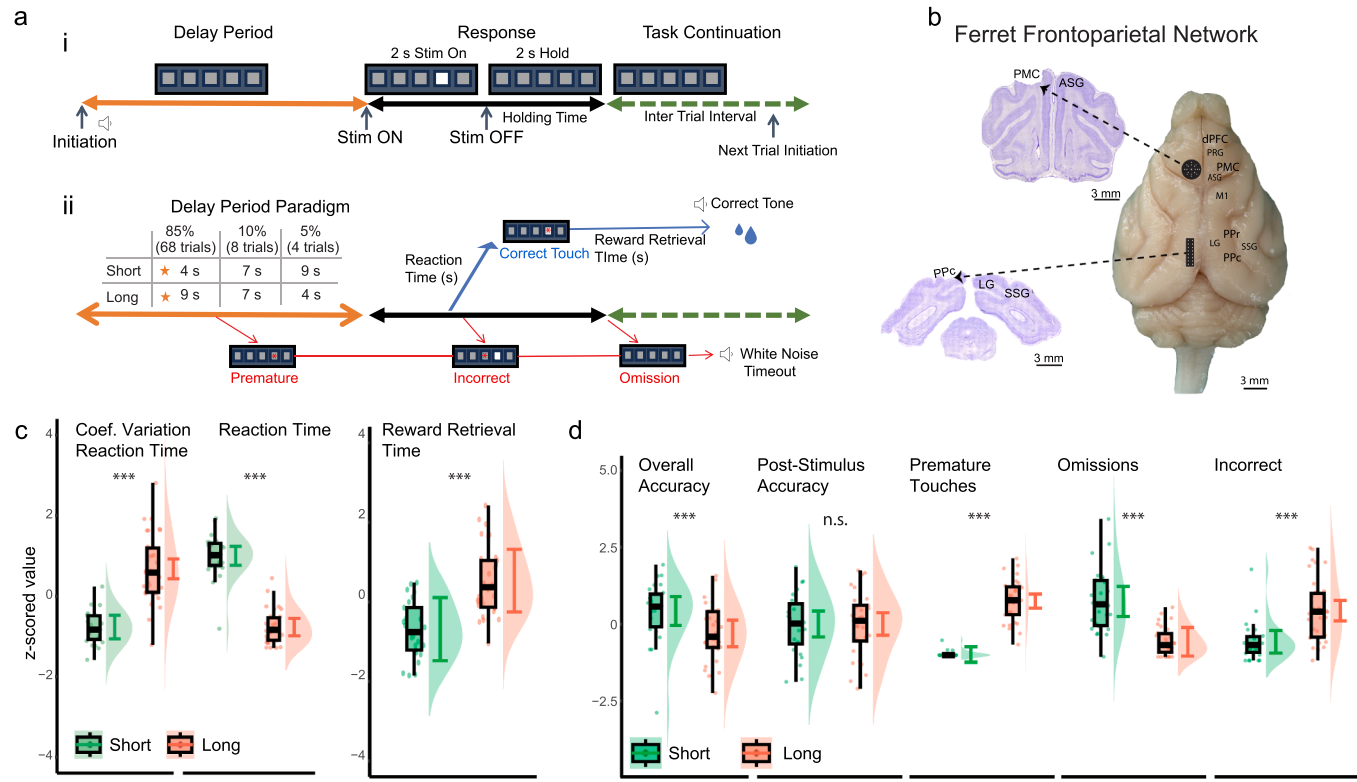


Fig. 1. Longer delay period in the 5-CSRTT degrades attentional performance across behavioral outcomes and histological verification of anatomical targeting. (a) Illustration of the three primary stages of the 5-CSRTT (i) and a description of our paradigm for manipulating delay length with potential trial outcomes indicated (ii). Subsequent data analysis includes only trials of the principal delay length (marked by orange stars in *Delay Period Paradigm* table) for each task condition. Coefficient of variation: std dev/mean * 100. (b) Example Nissl-stained sections of premotor (top) and posterior parietal cortex (bottom) brain sections with anatomical labeling adapted from the ferret brain atlas (Radtke-Schuller, 2018). Scale bars included in the figure. The premotor and posterior parietal cortices are anatomically connected and make up the frontoparietal network in the ferret (Sellers et al. 2016). (c) Comparison of time-based behavioral metrics between short and long-delay sessions. Reaction time is measured from visual stimulus onset to correct touch. Coefficient of variation of reaction time describes how much reaction time varies across trials, within session (standard deviation/mean*100). Reward retrieval time describes the time lapsed after a correct touch and water reward collection. (d) Comparison of task performance outcomes between short and long-delay sessions. Overall Accuracy represents percent correct trials over all trial outcomes (correct trials / correct + premature + omission + incorrect), whereas Post-Stimulus Accuracy represents percent of trials where the stimulus is accurately detected (correct trials / correct + omission + incorrect). All other non-correct trial outcomes are calculated as a percentage which includes all trial outcomes (i.e., omissions / omissions + incorrect + premature touches + correct). Across measures in c and d, each dot represents data averaged across the principal delay length (short; 4 s, long; 9 s) from one session. A linear mixed effects model was built for each measure. Task condition and test day were included as predictors and random effects between animals and variations across test days were accounted for (ex: Measure ~ Condition (1 + Day | Animal ID, see *Supplemental Table 1&2* models 1–8). Real data is illustrated in boxplots, where violin plots show the distribution of model predicted data. Outliers greater or less than 3 standard deviations are removed. Data is z-scored prior to statistical testing. P-values adjusted for multiple comparisons with Holm-Bonferroni correction. *** p < 0.001.

next sought to identify how attention varied across trials, and calculated the coefficient of variation for reaction time (standard deviation/mean * 100), a marker of attentional optimality reported in human SA literature (Esterman et al., 2013; Esterman and Rothlein, 2019; Epstein et al., 2011). We found that animals exhibited higher variation in response times in the long-delay sessions compared to the shorter delay (mean: short 31.80 vs long 52.7, $p < 0.001$; Fig. 1c).

In summary, a longer delay period increased attentional load, as demonstrated by greater variation in reaction time across trials, in comparison to a shorter delay period.

2.2. Higher attentional load elicits significant changes in dFPN narrow band oscillatory activity

After establishing that our task manipulation significantly degraded behavior, we sought to assess the underlying effects of increasing attentional load on cortical oscillations. Specifically, we recorded the local field potential (LFP) from two nodes of the dFPN, a functional hub for orchestrating communication between brain regions in order to meet task relevant demands ((Marek and Dosenbach, 2018; Sellers et al., 2016); Fig. 1b). The frontal and parietal node of the ferret dFPN have

been anatomically and functionally defined as the premotor cortex (PMC) and posterior parietal cortex (PPC) (Ross et al., 2024; Sellers et al., 2016). Narrow-band oscillatory power was isolated (theta (4–7 Hz), alpha (16–19 Hz), gamma (56–59 Hz)) from each node and averaged across trial delay within session, then averaged over sessions within condition (i.e., short or long-delay) (see *Methods*). Given that our task is self-paced and continuous, there is no rest period between trials that could serve as a true baseline to contrast neural responses during task performance. As such, we report non-baseline normalized results, however we exploratively visualized how neural activity during the delay period was different from the time period immediately prior to task initiation (see *Supplemental Discussion Section 1, and Supp. Fig 3*). We compared both average power spectral density (PSD) (*Supp. Fig 1*) and slope, which described the change in power over the delay period (*Supp. Fig 2*) of each frequency of interest between task conditions (see *Methods*). Specifically, we assessed frontal and parietal theta, alpha and gamma oscillations, based on their established roles in the coordination of attentional resources and attentional orientation, regulating cortical excitability and activation of task-relevant activity, respectively (Clayton et al., 2015; Huang et al., 2024; Lundqvist et al., 2020; Qu et al., 2024).

Given that previous work reported a reduction in frontal theta power during prolonged cognitive engagement (Yu et al., 2022), we predicted a reduction in frontal theta power throughout the long-delay. We did find that frontal theta power significantly decreased throughout both delay conditions (short; $p < 0.001$, long; $p < 0.001$). More importantly, power decreased significantly more in the long compared to short-delay condition, across animals ($p < 0.001$, two-tailed Wilcoxon signed rank test; Supp. Fig. 2a). Average frontal theta power during the delay was not significantly different between short and long-delays ($p = 0.87$; Supp Fig. 1a). We next assessed frontal gamma power during the delay period (56–69 Hz). Average frontal gamma power was also not significantly different between short and long-delays ($p = 0.912$, Supp Fig. 1b), but did increase throughout the long-delay more significantly ($p < 0.001$; Supp Fig. 2b). Lastly, we analyzed frontal alpha oscillations, which have been implicated in top-down inhibitory gating of sensory information (Minami et al., 2023; Lustenberger et al., 2016). We found that frontal alpha power did not change significantly throughout long ($p = 0.58$) or short-delay period ($p = 0.13$, Supp Fig. 1c). Similarly, frontal alpha power was not significantly different from zero for either task condition (long: $p = 0.58$, short: $p = 0.13$, Supp Fig. 2c). We additionally did not find any differences between task condition for average frontal alpha power ($p = 0.86$) or change in frontal alpha throughout the delay ($p = 0.45$).

We next sought a similar characterization of LFP in the parietal node of the dFPN (Fig. 3). We predicted parietal theta and gamma power would increase as the delay extended in long-delay trials, indicating the integration of information across multiple sensory modalities to support behavioral performance under higher vigilance demand. As expected, we did find an increase in both theta ($p < 0.001$; Supp Fig. 2c) and gamma power ($p < 0.001$; Supp Fig. 2d) throughout the long-delay that was not observed in the short-delay ($p = 0.206$; Fig. 3b, $p = 0.545$). Mean PSD was not significantly different between conditions for theta ($p = 0.206$; Supp Fig. 1c) or gamma ($p = 1.00$; Supp Fig. 1d). In line with previous findings (Huang et al., 2024), we demonstrated a reduction in alpha power throughout the delay of both 5-CSRTT conditions ($p < 0.001$, Supp Fig. 2e). However, there was a greater reduction in alpha power in the long-delay condition when compared to the short-delay ($p < 0.001$). There was no difference in mean alpha power between conditions ($p = 0.111$; Supp Fig. 1e).

After establishing higher attentional load induced changes to average oscillatory activity in PMC and PPC, we aimed to better understand when these changes occur. Attentional load was expected to be equivalent between task conditions until the duration of the long-delay exceeded the duration of the short-delay, 4 s after initiation. We then hypothesized that if changes in LFP are induced by increased attentional load, significant changes in oscillatory activity would occur around 4 s following initiation of long-delay trials. Our power spectrogram results visually support this hypothesis. We then calculated the time of the largest change in activity for each frequency band of interest in long-delay trials. Aligned with our hypothesis, we found that the largest reduction in frontal theta power occurred at $4.3 \text{ s} \pm 1.0$ and the largest increase in gamma power occurred $4.1 \text{ s} \pm 2.3$ following trial initiation. Considering PMC and PPC are both structurally and functionally connected, we predicted a similar timeline of oscillatory changes in the parietal cortex. Indeed, the largest increase in parietal theta occurred $4.7 \text{ s} \pm 0.57$ after initiation, closely aligned to reduction in alpha ($4.4 \text{ s} \pm 0.81$ after initiation) and increase in gamma ($4.3 \text{ s} \pm 1.1$ after initiation). Thus, significant changes in oscillatory band activity within PMC and PPC are temporally aligned to when the two task conditions diverge.

2.3. dFPN undergoes a significant state change four seconds after initiation in long-delay trials

After finding that the most significant change in power of individual frequency bands occurs ~ 4 s after trial initiation in the long-delay task, we compared the first 4 s of long-delay trials to the entire 4 s short-

delay. This comparison represents the time window between tasks that we predicted attentional load to be the same, and thus hypothesized neural activity would be similar. To test this hypothesis, we used non-parametric permutation testing to determine the significance of the LFP difference between the two delay conditions. As predicted, there were no significant differences in LFP for either PMC (Supp Fig 4a) or PPC (Supp Fig 4b) between the short-delay and first 4 s of the long-delay.

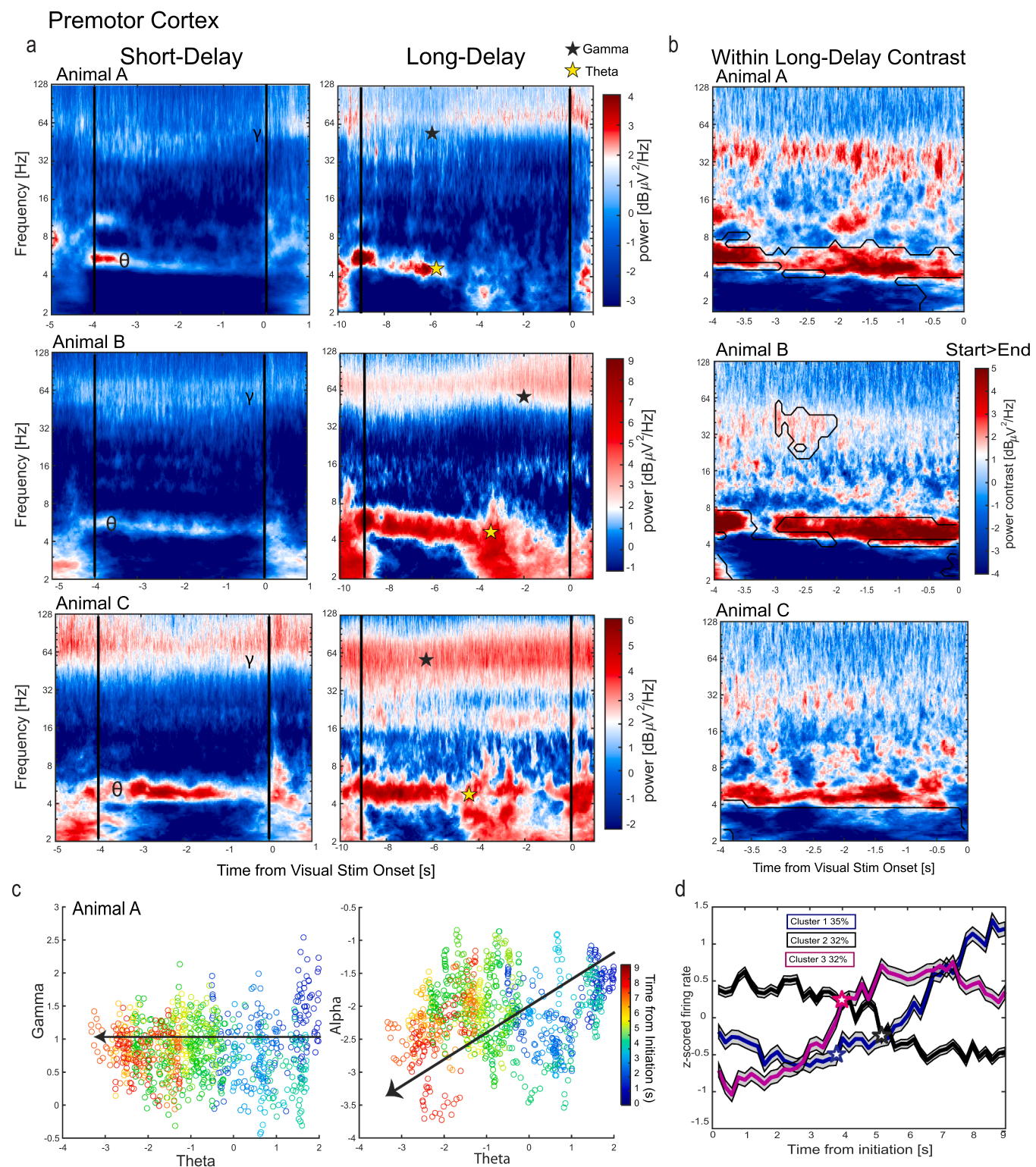
We observed that frontal theta power is higher at the beginning of long-delay trials compared to short-delay trials, although this difference is not statistically significant (Supp Fig. 4). This observation supports our claim that the attentional demands placed on the animals differ between short and long-delay trials, as increased attentional demand is associated with increased frontal theta power (Clayton et al., 2015; Jensen and Mazaheri, 2010). Given this association, our data suggest that the elevated frontal theta power in long-delay trials reflects greater behavioral demand. This increased recruitment of frontal theta power may also contribute to faster resource depletion, aligning with the heightened cognitive effort required for long-delay trials (Supp Fig. 4). We then repeated permutation testing to contrast LFP between the first and last 4 seconds of the long-delay. This analysis directly contrasts two time windows where attentional load is hypothesized to be higher (second half) than the other (first half) and result in unique neural activity. Results from this contrast demonstrated a significant reduction in frontal theta power in the second half of the long-delay (Fig. 2b). In the PPC, alpha power significantly decreases while theta and gamma power increase in the second half of the long-delay (Fig. 3b).

The relationship between frequency bands was plotted to visualize state change in each region. In the PMC, the most significant change in LFP is a reduction in theta power (Fig. 2c). In the PPC, theta, alpha and gamma have distinct relationships that are organized by time. Specifically, during the long-delay, alpha decreases while theta and gamma power increase (Fig. 3b).

In summary, we demonstrate a shift in dFPN oscillatory dynamics as attentional load increases in our long-delay task during the last four seconds, characterized by a reduction in frontal theta and parietal alpha, and an increase parietal theta and gamma power.

2.4. Single units in the PMC exhibit unique task-modulated firing patterns and are influenced by attentional load

After identifying significant LFP fluctuations in the second half of the long-delay, we investigated how attentional load influenced dFPN activity at higher spatial resolution and analyzed activity from PMC single units. We hypothesized that single units in the PMC would fire preferentially to task-demands, in line with previous reports in visual discrimination tasks (Zhou et al., 2016), and be modulated by attentional load. To address these hypotheses, we computed peristimulus time histograms (PSTHs) for all isolated single units in the PMC (see Methods) during the long-delay period. Data was grouped across three animals (Huang et al., 2021). For each task condition, PSTH's were pooled and clustered. Overall, we found that single units either responded more to task initiation and decreased in activity throughout the delay, or started with low activity that increased in anticipation of the visual stimulus onset (Fig. 2d). We identified two subtypes of single units that fired more in anticipation of the visual stimulus. One subtype showed a continuous increase in activity leading up to the visual stimulus, while the other increased in activity then plateaued during the second half of the long-delay. The largest change in frontal single unit firing rate in long-delay sessions occurred at 3.8 s, 5.2 s and 4 s following task initiation for clusters 1–3, respectively. These findings demonstrate task-modulated specificity in single unit firing patterns, which are disrupted approximately 4–5 s following task initiation, aligning with significant changes observed in LFP results.



(caption on next page)

Fig. 2. Longer SA delay period elicits changes in local field potential and single unit dynamics in the premotor cortex. (a) Power spectrogram of LFP in the PMC from trial initiation (first vertical black line) to visual stimulus onset (second vertical black line) for short (left) and long-delay (right) behavioral sessions for animals A-C. Spectral data is averaged across principal delay length trials within session and then averaged across sessions. The aperiodic component (APC) is removed from group-averaged data, then subtracted from each session. After APC subtraction, data is re-averaged. Location of black and yellow star denotes change point for gamma (56–59 Hz (γ)) and theta (4–7 Hz (Θ)) band power, respectively. Greek letters visually mark the location of frequencies of interest. (b) The difference in narrow band oscillatory power within the long-delay was analyzed. Plotted power spectrograms represent the LFP power difference between the first four seconds after trial initiation and last four seconds of trial leading up to visual stimulus presentation in long-delay. Statistically significant ($\alpha = 0.05$) differences between first and second half of the long-delay were calculated from non-parametric permutation testing and visualized with black contour. (c) Visual representation of the relationship between theta and gamma power (left), and theta and alpha power (right) throughout long-delay trials for Animal A. Each dot represents averaged (across trials then sessions) power of frequency one (x-axis) and frequency two (y-axis) at each time point throughout nine second delay (100 Hz sampling rate). A black arrow is overlayed to help visualize the trend of the two plotted frequencies over the time of the delay period, the arrow direction indicates start of trial to visual stimulus onset. (d) Spiking activity of 3 distinct clusters of single units recorded in PMC during the long-delay period in long-delay sessions. Single units were obtained from PMC electrophysiological data (see *Methods*). Peristimulus time histograms were obtained for every identified single unit for the delay period of long-delay behavioral sessions (200 ms time bins). K-means clustering was calculated to identify 'k' distinct, non-overlapping groups of the dataset, where $k = 3$. Percentage values by each cluster represent percentage of how many identified single units belong to each cluster. For power spectrograms in (b), statistically significant ($\alpha = 0.05$) differences between first and second half of the long-delay were calculated from non-parametric permutation testing and visualized with black contour. Total number of identified single units for short and long-delay sessions are 114 and 246, respectively. White-filled stars for long-delay sessions identify the time of largest change in mean and slope for each cluster after task initiation (Cluster 1: 3.8 s, Cluster 2: 5.2 s, Cluster 3: 4 s).

2.5. Animals become increasingly engaged with the visual stimulus windows as SA delay progresses

To relate our neural findings to animal behavior, we employed a deep-learning based computer vision tool (DeepLabCut) to track animal head position during the long-delay (Nath et al., 2019; Mathis et al., 2018). Specifically, we calculated velocity within the whole long-delay period (Fig. 4a), and quantified head position at 3 s, 5 s, and 8 s after initiation for animals A-C (Fig. 4c-e). The selection of time points for head position analysis was motivated by the velocity results, aiming to capture unique phases of behavior throughout the delay and provide insight into individual animal strategies for task completion (Fig. 4b). Overall, animals A-C displayed very similar behavioral strategies. Animals were relatively static for the first 4 s of the delay, then began moving quickly between 4 and 7 s and maintained activity during the last two seconds before visual stimulus onset. Spatial maps of animal head position showed that animals remained at the initiation location 3 s after initiation, were moving towards the visual stimulus windows at 5 s and scanned the stimulus windows at 8 s. These results suggest that animals are relatively static before the change points in LFP and SU data, then became actively engaged in searching for the visual stimulus afterward. However, we do not predict that animal locomotion accounts for, or affects our neural results (see *Supplemental Discussion Section 2*).

We additionally analyzed behavior during the short-delay sessions (Supp Fig. 5). Head position was quantified at 1.5 s, 2.5 s and 3.5 s following trial initiation (Supp Fig. 5b). In short-delay sessions, animals began the trial relatively stationary at the initiation location then begin approaching the visual stimulus screen about halfway through the trial, similar to pattern identified in long-delay sessions. However, there is more variety in animal strategy in the short-delay condition than was observed in the long-delay condition. For example, the analysis of velocity of head movement in the delay period of correct short-delay trials suggests that Animal B moved from the initiation location and began approaching and scanning the visual stimulus screens one second after trial initiation, earlier than Animal A and C, who remain at the initiation spout for 3 s (Supp Fig. 5a). Additionally, Animal B's velocity continuously increases from 2 to 4 s after initiation, whereas Animal A and C increase velocity in the final second of the short-delay. Spatial maps of animal head position confirm that overall, animals are at the initiation location 1.5 s after trial initiation, begin moving towards the visual stimulus screens 2.5 s after trial initiation and then start scanning visual stimulus screens 3.5 s after trial initiation (Supp Fig. 5c). These results suggest animals have a similar behavioral strategy for task completion between short and long-delay sessions.

In long-delay sessions, animals respond to the visual stimulus significantly faster than in short-delay sessions, potentially reflecting heightened task engagement. To further investigate the animal's

preparedness to respond in long-delay trials, we analyzed distance from the initiation spout at time of visual stimulus onset. We found that animals are further away from the initiation location (i.e., physically closer to the visual stimulus screens) in the long-delay condition (two-sample *t*-test, $p < 0.001$). This result suggests that proximity to the visual stimulus screens is part of the animal's strategy for completing the task under high attentional demands, reflecting heightened engagement in the long-delay condition as animals are prepared to respond but actively inhibit their reaction.

2.6. dFPN functional connectivity desynchronizes during long SA delay

To provide a potential causal explanation for why performance is degraded with higher attentional load, we analyzed how network functional connectivity changes during the task. Considering our observation that frontal theta was significantly reduced during the long-delay task, we predicted a reduction in network connectivity with high attentional load at a similar time point. To test this, we measured functional connectivity via phase locking value (PLV), and confirmed that dFPN synchronization was centered at theta and task modulated (Fig. 5a). Specifically, average theta-PLV was positive and significantly greater than zero in both task conditions (long & short $p < 0.001$), while significantly more positive in the long-delay condition ($p = 0.03$; Fig. 5b). Granger Causality was then calculated and averaged over theta frequency (4–6.5 Hz) to assess direction of the identified theta phase connectivity and found to be primarily top-down (PMC->PPC) during the delay of both task conditions (short; $p < 0.01$, long; $p < 0.05$, Fig. 5c). As initially predicted, the change in theta-PLV throughout the long-delay task was negative and significantly different from zero ($p < 0.001$; Supp Fig. 2g). This finding was different from the short-delay condition ($p < 0.001$), where change in theta-PLV was not significantly different from zero ($p = 0.393$). We then calculated the time of the largest change in theta-PLV and found it to be $5.1 \text{ s} \pm 0.32$ into the long-delay. This timing is notable, as it aligns with the changepoints previously calculated for LFP and SU data as well as a change in animal behavior from static at initiation location to moving towards the stimulus windows.

2.7. Reduced dFPN theta connectivity selectively impairs sustained attention

Finally, we aimed to identify if the observed reduction in theta-PLV was a neural correlate of the decline in attentional performance observed in the long-delay task. We hypothesized that if dFPN theta-connectivity is required for successful attentional engagement, then the desynchronization observed during the long-delay would be correlated with impaired attentional performance. To test this, we assessed

Posterior Parietal Cortex

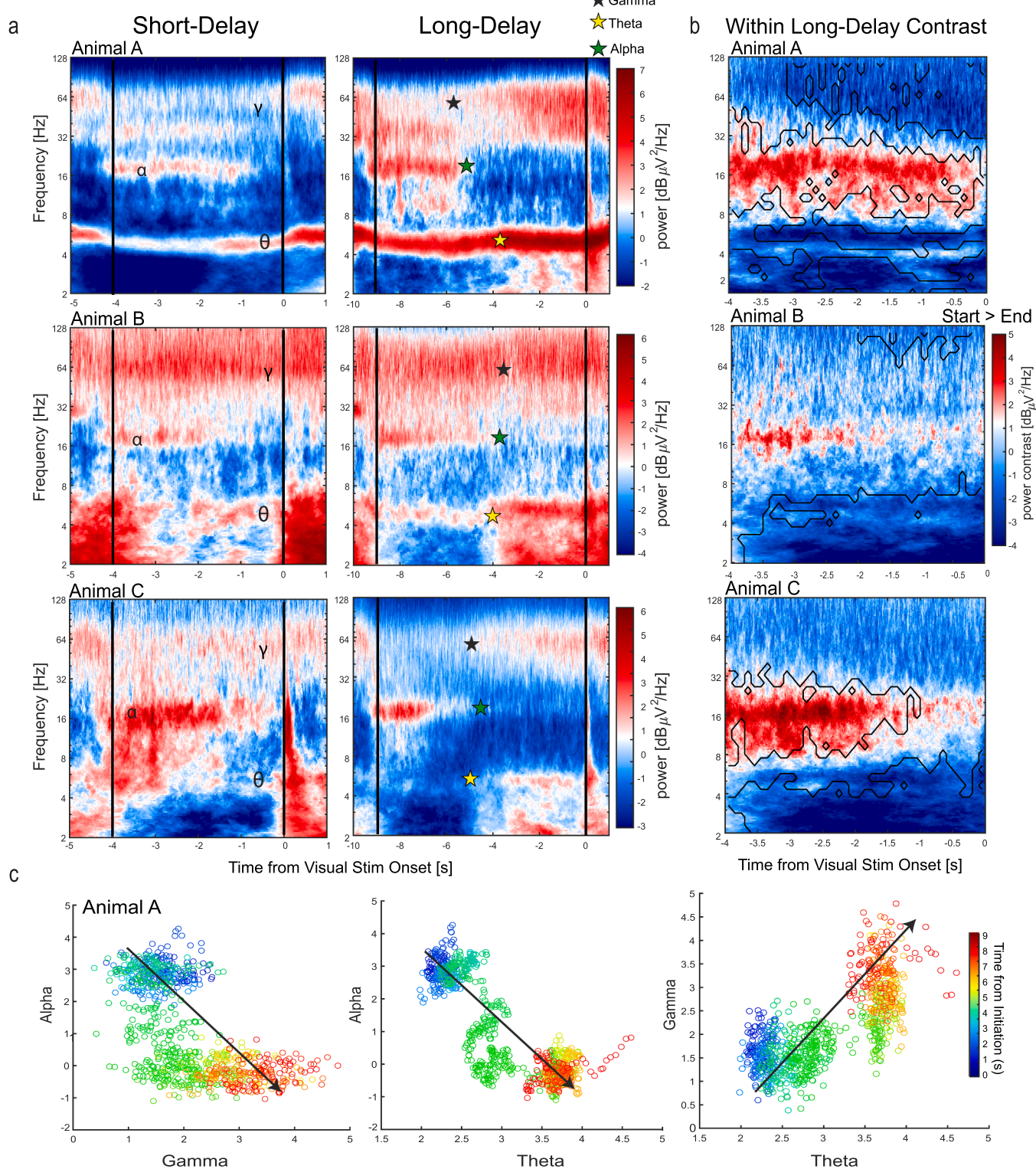


Fig. 3. Parietal alpha power reduces, while theta and gamma power increases throughout the longer SA delay period. (a) The difference in narrow band oscillatory power in PPC during the long-delay was analyzed. Method identical to that described in Fig. 2b, repeated for PPC LFP. Statistically significant ($\alpha = 0.05$) differences between first and second half of the long-delay were calculated from non-parametric permutation testing and visualized with black contour. (b) Visual representation of the relationship between alpha and gamma power (left), theta and alpha power (middle) and gamma and theta (right) power throughout the long-delay for Animal A. As for Fig. 2c, each dot represents averaged (across trials then sessions) power of frequency one (x-axis) and frequency two (y-axis) at each time point throughout nine second long-delay (100 Hz sampling rate). A black arrow is overlaid to help visualize the trend of the two plotted frequencies over the time of the delay period, the arrow direction indicates start of trial to visual stimulus onset.

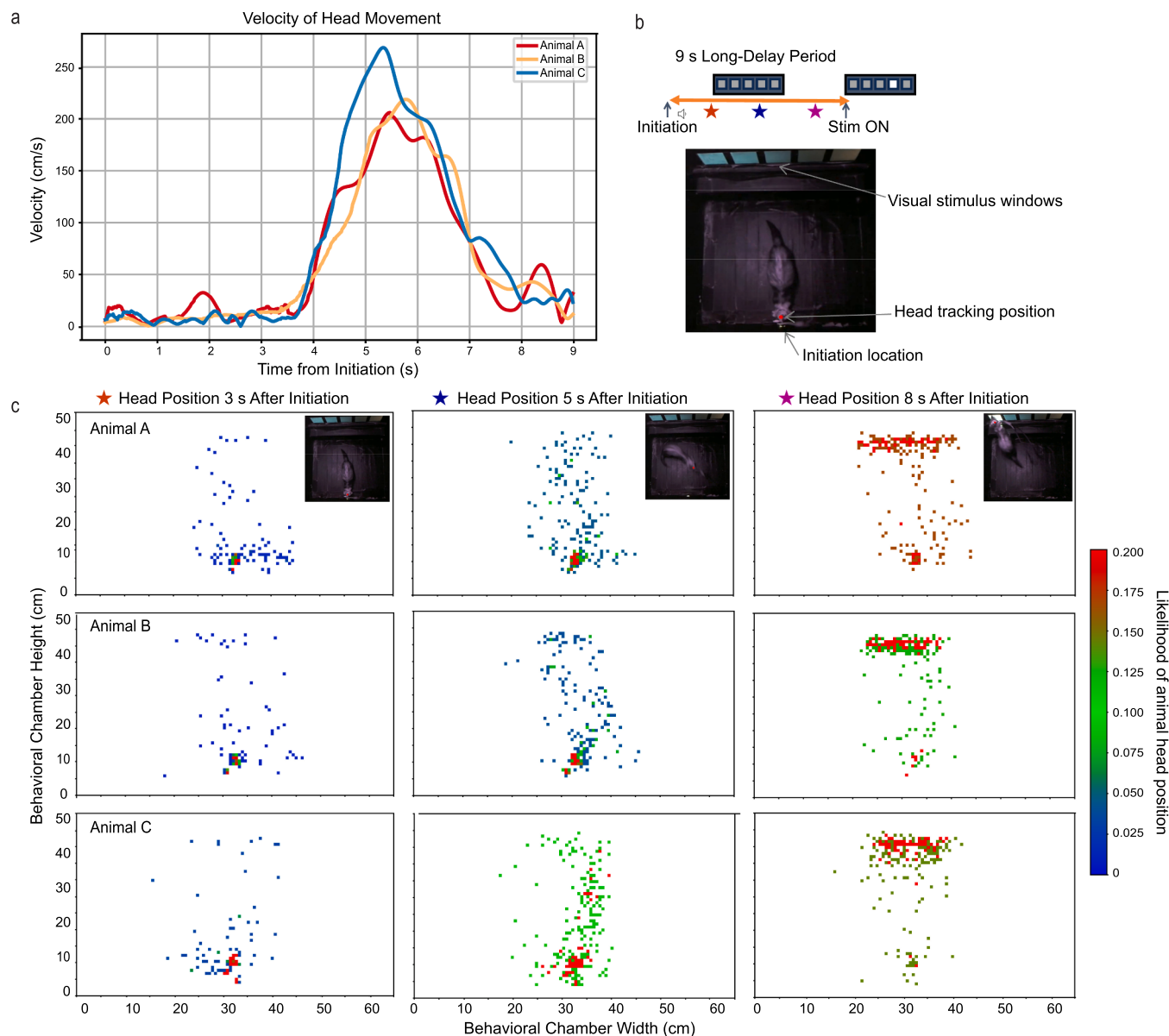


Fig. 4. Animals display consistent behavioral strategy for task performance when attentional load is high. (a) Velocity of animal head movement throughout the delay period of long-delay trials aligned to trial initiation. Animals remain relatively static the first 4 s after initiation then begin to move rapidly 4–7 s and have relatively sustained activity in the last 2 s of the delay. Reported velocity is an average across the delay period of correct trials in long-delay behavioral sessions. (b) Experimental design. (top) The likelihood of animal head position within the behavioral chamber was calculated for three timepoints after trial initiation, 3 s (orange star), 5 s (blue star) and 8 s (purple star). (bottom) Frame from experimental video illustrating the annotation of ferret head position analyzed by DeepLabCut and location of task relevant chamber features (i.e., initiation location, visual stimulus windows). (c) Two-dimensional histogram of animal head position was generated at specific time points of the SA delay period in long-delay sessions of the 5-CSRTT for animals A-C. The histogram was calculated with position data generated in DeepLabCut from frames of correct trials performed by each animal. Representative frames from the annotated behavioral video of the most likely animal head position in the behavioral chamber are included for each time point in upper right corner. Animal A, B, C completed 247, 271, and 285 correct trials respectively. Histogram values are normalized to total trial number. Bin size 0.55 cm².

the relationship between change in theta-PLV over the delay period and the coefficient of variation of RT (CV-RT), a marker of attentional optimality reported in human SA literature (Esterman et al., 2013; Esterman and Rothlein, 2019; Epstein et al., 2011). We first established that increased variability in RT is observable in the long-delay task (Fig. 1c), reflecting poorer attentional performance with increased attentional load. Next, utilizing a mixed model, we found that inclusion of the change in theta-PLV throughout delay (ANOVA; $p = 0.002$) and task condition (ANOVA; $p < 0.001$) as predictors significantly improved the model for CV-RT (Fig. 6a). Importantly, inclusion of change in theta-PLV throughout the delay did not significantly improve the linear

mixed model for premature (ANOVA; $p = 0.08$) or incorrect (ANOVA; $p = 0.30$) trials, indicating that change in theta-PLV does not specifically predict attention fluctuations. We next explored the relationship between change in theta-PLV and CV-RT with Spearman correlation, and found a weak, near-significant negative relationship in the long-delay condition ($r = -0.327$, $p = 0.06$) that was not observed in the short-delay condition ($r = 0.125$, $p = 0.56$). Together, these results suggest that variation in RT, a marker of suboptimal attention reported in human studies, increases as theta-PLV decreases in our higher attentional load condition.

In human studies, SA is assessed by the coefficient of variation of RT

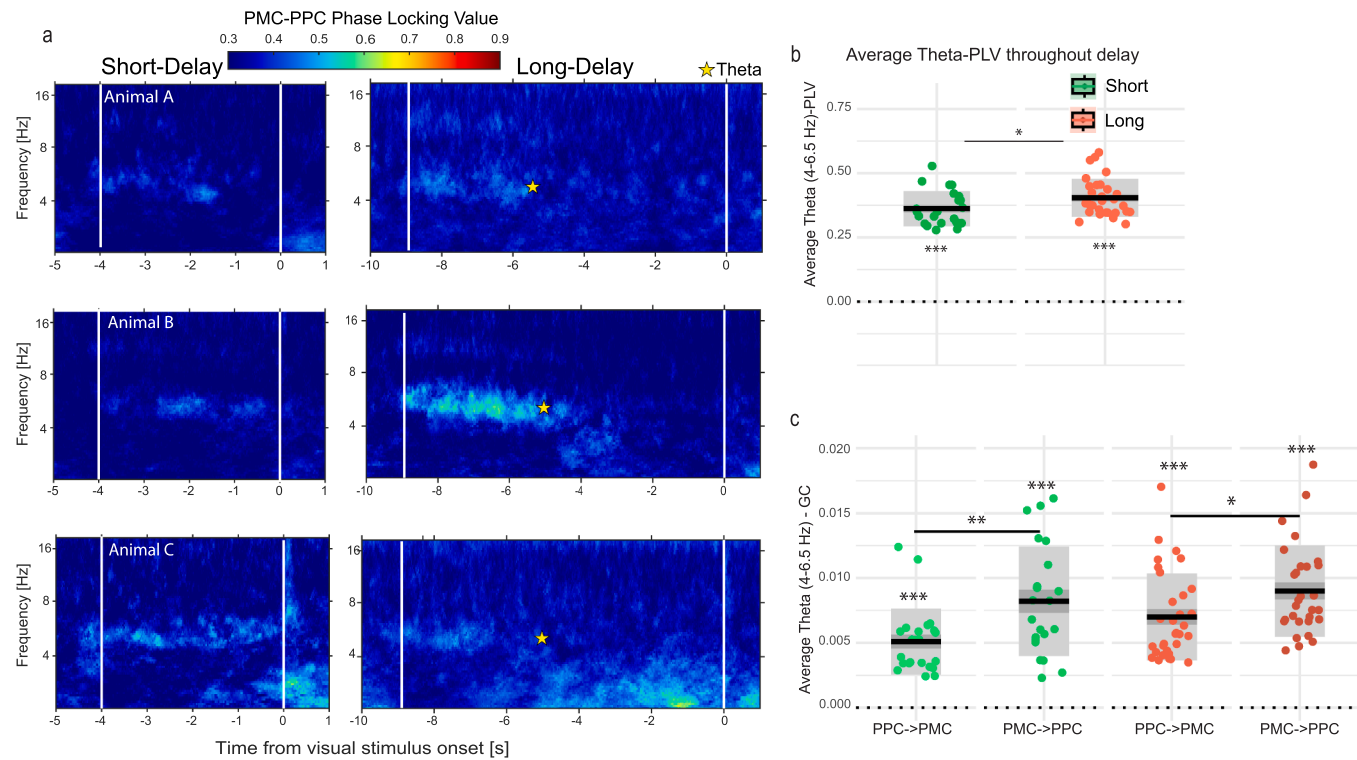


Fig. 5. Top-down theta functional connectivity of the frontoparietal network degrades in longer SA delay. (a) PLV was the primary measure of functional connectivity, and was calculated within short (left) and long-delay (right) trials for animals A-C. The first and second vertical white lines mark trial initiation and visual stimulus onset. Yellow star denotes largest change in theta band (4–6.5 Hz) PLV in the long-delay. (b) Theta band (4–6.5 Hz) PLV was quantified throughout the short and long-delay period for animals A-C. (c) Theta band (4–6.5 Hz) Granger Causality results for short and long-delay (Animal A-C combined). For (b-c) significance ranking above two bar plots with horizontal black bar denotes significant difference between short and long-delay conditions, whereas significance ranking without the black bar represents how different the values within condition are from zero. Shaded dark grey denotes SEM, shaded light grey denotes SD, black bar is mean across sessions and subjects, dotted line marks zero. * $p < 0.01$, ** $p < 0.05$, *** $p < 0.001$, two-tailed Wilcoxon signed rank test. GC: Granger Causality, PLV: phase locking value.

(CV-RT), while in animal studies, mean RT is used to gauge task engagement. We next sought to identify if the relationship between theta-PLV and CV-RT was specific, or if it extended to mean RT as well. We accomplished this by repeating our correlation tests on mean RT, in place of CV-RT. Utilizing a mixed model, we did find that slope of theta-PLV (ANOVA; $p = 0.008$) and condition (ANOVA; $p < 0.001$) as predictors improved the model for predicting mean-RT (ANOVA; $p = 0.008$), as we observed with CV-RT (Fig. 6b). However, no relationship was found between mean RT and slope of theta-PLV with Spearman correlation tests, in either condition (long; $r = -0.08$, $p = 0.63$, short; $r = 0.067$, $p = 0.76$).

Finally, we tested how well CV-RT and mean RT predicted change of theta-PLV. We found that inclusion of CV-RT (ANOVA; $p = 0.04$), but not mean-RT (ANOVA; $p = 0.283$), improved our model for predicting slope of theta-PLV (Fig. 6c). Together, our results suggest that stability of theta-PLV is weakly negatively correlated with RT variability when attentional load is high.

3. Discussion

The present study provides the first evidence of how attentional load influences ongoing oscillatory dynamics of the dFNP. Attentional load was strategically manipulated within trials of the 5-CSRTT and resulted in significant session level changes in attentional performance. Our task design enabled us to directly contrast narrow-band oscillatory activity, functional connectivity and SU dynamics within the dFNP between high- and low-attentional load conditions. Across all measures, we identified a significant change in activity temporally aligned to an increase in attentional load. Our neurophysiology results align with behavioral

annotation which suggests that at the start of the SA delay period, animals are in a static, internally focused state which requires top-down control then shift to a state of sensory integration as animals begin approaching and scanning the visual stimulus windows. Finally, we identified a brain-behavior relationship which suggests the extent to which theta-band dFNP connectivity is sustained during task performance predicts attentional variability.

3.1. Animals shift from internally focused top-down task preparation to visual stimulus scanning and sensory integration

The present results demonstrate a consistent across-animal behavioral and neurophysiological strategy for completing a SA behavioral task when attentional load is high. This strategy includes a distinct shift in neural activity of the dFNP from top-down signaling to integration of sensory information when animals begin exploring the location of the visual stimulus. Our work addresses a gap in current attention theory which has been primarily focused on selective attention as a function of perceptual and cognitive load (Lavie, 1995; Lavie and De Fockert, 2005; Lavie and Tsal, 1994; Murphy et al., 2016). Attentional load differs importantly from cognitive load, which is not specific to attention but describes all demands on cognitive processing (Demirayak et al., 2023) and perceptual load, which describes the amount and complexity of incoming sensory information (Lavie and Polly 2014; Nobre and Sabine Kastner, 2014). In our task design, we increased attentional load by lengthening the period of time an animal must remain engaged in the task, and observed distinct shifts in LFP and SU activity influenced by load. Our observations have multiple implications. One possibility is that the observed state shift in the dFNP reflects an effort to conserve

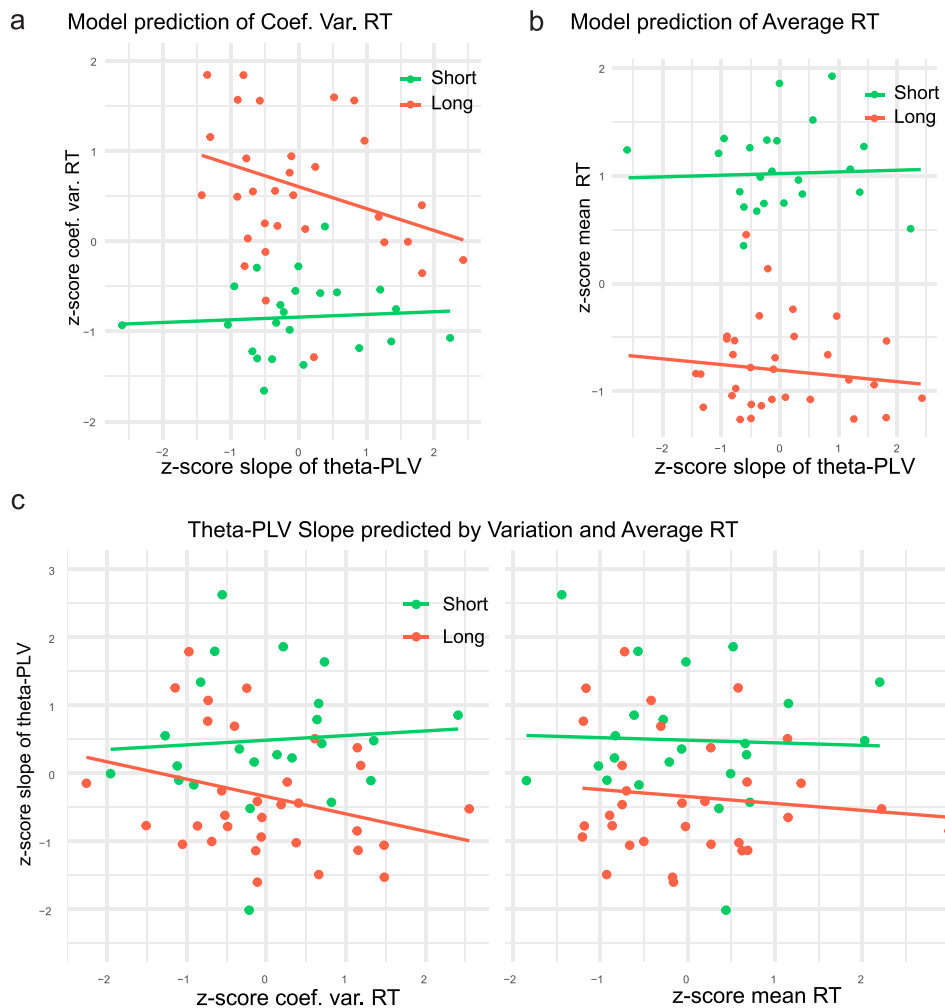


Fig. 6. Reduction in frontoparietal theta connectivity correlates to more variable responses during longer SA period. (a) Model prediction of coefficient of variation from theta-PLV slope. ($\text{Coef. Var} \sim \text{Theta-PLV Slope} * \text{Condition} + (1 + \text{Day} | \text{AnimalID})$). (b) Model prediction of average reaction time from theta-PLV slope. ($\text{Mean Reaction Time} \sim \text{Theta-PLV Slope} * \text{Condition} + (1 + \text{Day} | \text{AnimalID})$). (c) Model prediction of theta-PLV slope by coefficient of variation of reaction time and mean reaction time. ($\text{Theta-PLV Slope} \sim \text{Coef. Variation RT} + \text{Average RT} + (1 + \text{Day} | \text{AnimalID})$). For (a-c) each dot represents one session averaged data. Data from animals A-C are included. See [Supplemental Tables 1 & 2](#) (models 8–11) for building of mixed models and report of model fit.

attentional resources. The reported reduction in frontal theta power suggests a depletion of cognitive resources (Yu et al., 2022; Baumeister et al., 1998; Nielsen et al., 2001; Webster et al., 1996), indicating that a shift towards parietal sensory integration may be required to remain engaged in the task after frontal resources are exhausted.

It is also possible that the role of the dFNP is only required at the initiation stage of the task and the brain dynamically shifts to different network states that involve the PFC for sustained task engagement. This conclusion is supported by studies which report that SA requires dynamic shifting and integration of other neural networks including the default mode network (Esterman et al., 2013; Seeburger et al., 2024) and cinguloopercular network (Dosenbach et al., 2007), among others (Seeburger et al., 2024), suggesting that additional neural networks could be recruited following the dFNP. Further, frontal theta band activity typically supports the initiation and execution of cognitive control, though its role may change depending on specific cognitive control strategies (Eisma et al., 2021; Cavanagh and Frank, 2014). Therefore, it is possible that frontal theta is required for task initiation, but not for monitoring stimulus locations.

3.2. Top-down frontoparietal theta phase synchrony supports SA

In human research, SA is defined as variability in attentional

engagement over trials, measured through fluctuations in reaction time. In contrast, animal studies primarily assess task engagement using session-averaged outcomes, such as accuracy and overall RT. In this study, we assess how both trial-to-trial variations in RT (coefficient of variation) and session-averaged RT are influenced by attentional demand and their relationship to dFNP theta connectivity.

Increased attentional load has complex effects on RT, including faster average RT and greater variation in RT across trials, reflecting underlying cognitive processes and task engagement. A longer RT on average may reflect a slowdown of cognitive processing and thus disrupted SA (Fang and Frohlich, 2023). In an emotion processing task on human participants, researchers reported a slower average RT with increased attentional load (Liu and Ji, 2024). This result has been replicated in humans during a gradual-CPT task (Esterman et al., 2013) and in ferrets performing a visual discrimination task (Zhou et al., 2016). However, the latter task did not specifically probe attention, and interpreted the longer RT in the context of behavioral inhibition, suggesting that longer RT allowed for more careful decision making. In contrast, RT in our study does not represent the time to make a perceptual decision, but rather time to respond to an anticipated visual stimulus. Contradictory to the abovementioned reports, when we increased attentional load in the present study, we found a significantly shorter RT under conditions of high attentional load. However, our

finding does align with previous ferret research suggesting that a shorter RT reflects greater task engagement during the 5-CSRTT, which is necessary to meet greater attentional demands (Huang et al., 2024). We propose that a shorter RT in our task is reflective of the stress on response inhibition due to having to wait longer for the visual stimulus. This interpretation would suggest that animals are prepared to respond to the visual stimulus screen as soon as it appears, which we demonstrated by showing that animals are more likely to be at the stimulus windows than anywhere else one second prior to visual stimulus onset. There is also a greater occurrence of premature responses in the higher attentional load condition, indicating that if animals are able to resist reacting prematurely, they are primed to respond to the visual stimulus somewhat immediately.

The coefficient of variation for RT has been reported as a metric of vigilance in human SA research (Esterman et al., 2013; Gbadeyan et al., 2022; MacDonald et al., 2006; MacDonald et al., 2009), but to our knowledge has not yet been applied to animal studies. In human literature, greater variation in RT across trials within a SA behavioral session demonstrates greater moment-to-moment fluctuations in attention and suggests diminished attentional performance. In this context, our results show worsened SA performance under high attentional demand. However, we also found that average RT is faster when attentional demand is high, suggesting increased task engagement. These findings suggest that attentional state and task performance can differ. Meaning that an animal may be more engaged and attentive (i.e., faster RT) when attentional demand is high, even if task performance (i.e., lower accuracy, higher RT variation) is poorer, compared to when demand is low.

Time-based fluctuations in attention are linked to cortical oscillations in attention-related brain networks, including the dFPN (Clayton et al., 2015). To better contextualize our behavioral findings alongside our neurophysiological results, we examined the relationship between RT metrics and dFPN theta connectivity under high attentional load, which was hypothesized to be critical for sustaining attention. Our results indicate that greater variation in RT within a session negatively correlates with sustained theta PLV when attentional demand is high. Specifically, this suggests that more consistent dFPN theta connectivity during the long-delay period is associated with less variability in RT. Notably, we did not observe a significant relationship between RT variation and change in theta PLV throughout the delay under low attentional load. Observing a correlation between variation in RT and theta phase connectivity only in the high attentional load condition suggests a specific role of dFPN rhythmic connectivity in supporting 5-CSRTT performance when demand for attentional resources is high. The specificity of the role of dFPN theta connectivity is further exemplified by the fact that we did not observe a significant relationship between average RT and change in theta PLV. Meaning that under high attentional load, dFPN theta connectivity supports 5-CSRTT performance by reducing variability in RT across trials. The lack of relationship between average RT and theta connectivity further implies that RT speed may be influenced by distinct cognitive processes, possibly including inhibitory control.

3.3. Conceptualizing sustained attention in the modified 5-CSRTT

SA requires both inhibitory control and maintenance of task engagement (Reck and Hund, 2011; Chen et al., 2024). Our modified version of the 5-CSRTT successfully taxed the attention system, evidenced by an increase in premature touches and variation in reaction time. With this holistic perspective of SA, we propose that the reduction in overall task accuracy driven by premature touches demonstrates a breakdown of cognitive processes that contribute to SA. We aimed to examine neurophysiology in the dFPN in correct trials where animals must allocate attentional resources under higher demand achieved by the extended prestimulus delay. This approach differs from previous reports of SA which detail vigilance decrements over time as a sign of fatigue (Young et al., 2009), effects that were neither the aim of our

study nor observed. While vigilance decrements are one cardinal measurement of SA in human studies, reaction time variability is another, capturing moment-to-moment attentional fluctuations between trials (Esterman and Rothlein, 2019). We demonstrate increased fluctuations that map onto neural activity in the longer-delay task condition, indicating this is a more appropriate measurement of SA in our task context. Given the differential reaction times for the two task conditions, an alternative approach would be to consider absolute variability without normalization by mean reaction time. Future theoretical work and computational modeling will be needed to delineate the implications of this approach. Eliciting and measuring vigilance decrements preclinically is more commonly achieved in 5-CSRTT variants that include non-target trials, where signal detection theory calculations (e.g., sensitivity index) more robustly capture changes in attention performance (Barnes et al., 2012; McGaughy and Sarter, 1995; Riccio et al., 2001; Skinner and Giesbrecht, 2025). Future investigations, beyond the scope of the current study, are recommended to include non-target stimuli to probe these complementary facets of neuronal dynamics of SA.

Alternatively, independent of attentional mechanisms, the observed increase in premature responses could also be a result of the task design or internal timing and response biases. Specifically, animals may be responding prematurely more frequently in the long-delay task condition simply because there is greater opportunity to do so than in the short-delay. In this case, animals may be more prone to prematurely respond due to extensive initial training on a shorter delay period, a result of internal timing mechanisms. Alternatively, animals may strategically respond faster to minimize the time elapses to the next trial and associated potential reward. Overall, the current task design and condition contrast employed in this study likely does not fully isolate the construct of sustained attention, and alternative behavioral explanations cannot be fully excluded. Future refinements of this task can build on this work and will accelerate the understanding of the neuronal basis of cognitive control and its subdomains.

3.4. Implications

In this study, we introduce a novel manipulation of a preclinical SA task that significantly alters dFPN activity in relation to behavioral performance under varying levels of attentional load. A key implication of our findings is the potential to improve attentional performance by targeting theta-connectivity in the dFPN through external stimulation. Our results highlight the temporal dynamics of network connectivity, offering valuable insights into the optimal timing for interventions aimed at addressing attentional impairments. This timing is crucial, as the strength of endogenous brain oscillations is known to influence the brain's responsiveness to external interventions (Alagapan et al., 2016; Schmidt et al., 2014).

A key advantage of the current study is the ability to interpret our neural results in the context of freely moving behavior. Unlike tasks with a preexisting fixation point, the 5-CSRTT enables each animal to develop its own behavioral strategy when attentional load is low versus when it is high. Using computer vision tools we tracked animal head position during high attentional load trials and observed distinct behavioral states that corresponded with significant changes in dFPN theta, alpha and gamma power during the delay period, as well as task modulated clusters of premotor single units. Initially, animals remained relatively stationary at the trial initiation location, and frontal theta oscillations and theta-band phase synchrony were observed within the dFPN. Approximately 4–5 s after trial initiation, as the animals began to move towards the visual stimulus screens, frontal theta power, dFPN connectivity and parietal alpha power decreased, while theta and gamma power increased in the parietal cortex. This state persisted as the animals surveyed the screens, suggesting a shift from a planning phase to one requiring multi-sensory integration. By not requiring fixation, we capture naturalistic sustained attention strategies. Our velocity and head

position data indicate animals spend more time at the stimulus screens during longer delays. The broad velocity peak suggests animals do not alternate between the stimulus screens and other locations in the behavior chamber, but rather approach and continuously scan the screens until stimulus presentation. Altogether our findings suggest that frontal theta power, a limited cognitive resource, is engaged early on and then the network shifts to support the processing of sensory information, potentially as a strategy to conserve resources. Task performance (RT) is more stable when dFPN theta connectivity is sustained, suggesting that while a neural state shift under increased attentional load conserves resources, continuous connectivity supports superior SA. This study is the first to our knowledge to thoroughly annotate behavior during the 5-CSRTT in relation to neural activity, providing new insights into behavioral strategies under high attentional load. Moreover, the consistency in brain and behavior patterns across animals suggests that these findings may be replicated in a larger sample.

Here, we directly assess neural correlates of attentional performance to visual stimuli. However, attention to relevant stimuli and suppression of irrelevant stimuli are complementary processes essential for sustaining attention (Clayton et al., 2015). A human study using a version of the 5-CSRTT that includes non-target trials, specifically requiring response inhibition, found an increase in frontal theta only in target trials (Cavanagh et al., 2021). Suggesting that frontal theta activity specifically relates to the attentional aspect of SA rather than inhibitory control. Further, although our task does not include non-target trials, we were able to identify that changes in functional connectivity are specific to attentional fluctuations by correlating our neural results with variability in RT. By doing so, we also strengthen the translational implications of our finding by conceptualizing SA as fluctuations in behavior over time. We do, however, observe an increase in premature touches in our high attentional load condition, a common marker of weakened inhibitory control in animals (Fang and Frohlich, 2023). While we did not identify a correlation between network functional connectivity and premature responses, it is a possibility to investigate the neural signature of inhibitory responses in our task design, although beyond the scope of our current study.

3.5. Limitations

Like all scientific research, our study has limitations. First, given the curvature of the ferret cortex, we were unable to ensure all channels of our MEA targeted the same cortical layer. As we average data across MEA channels, we do not differentiate layer-specific oscillations. Secondly, for the purposes of analytical congruity, we did not titrate difficulty to each animal's ability. For this reason, we included animal IDs as a random effect in our mixed model. Thirdly, we are unable to rule out effects from other cortical and subcortical circuits. Both frontal and parietal cortices are large hubs that interact within many other cortical networks, and are influenced by subcortical structures. As such, we are only able to draw conclusions from the findings of PMC and PPC. Fourthly, while inclusion of non-target, or no-go trials (when a visual stimulus is presented on all five screens the animal must inhibit response) would provide a direct measurement of response inhibition, there are challenges to us implementing this in our study. For instance, it is not possible to separate a correct non-target trial from an omission without precise video tracking as both trial outcomes do not include a captured behavioral response. Additionally, while a variation of the 5-CSRTT that includes non-target trials is performed in rodents (Barnes et al., 2012; Young et al., 2009), the behavioral training protocol has not been developed in ferrets and requires additional troubleshooting that has not yet been explored. Fifthly, we recognize the overall number of single units identified is relatively low, this reflects the complexities of achieving a good signal to noise ratio in *in vivo* electrophysiology.

Lastly, analyzing the neural dynamics of non-correct trial outcomes (omissions, premature and incorrect touches) would provide a direct comparison of neural dynamics required for successful task

performance, however certain limitations in the current task design prevent a comprehensive analysis of non-correct trial outcomes. The primary limitation stems from an imbalance of trial numbers, as non-correct trials occur far less frequently than correct trials, making robust statistical comparisons challenging. More specifically, premature responses cannot be analyzed due to the event time-based structure of our analysis and the variability in premature trial durations. Omissions require additional detailed behavioral annotation as an omitted trial may result from an animal not moving quickly enough (due to short-delay periods) rather than task disengagement. Incorrect trials, often attributed to decision-making errors, occur when an engaged animal selects a non-stimulus window.

3.6. Conclusion

The present study represents a significant step forward in understanding the neural mechanisms underlying SA. Here, we show a distinct shift in dFPN activity as attentional demands increased, marked by a reduction in dFPN theta connectivity and an increase in parietal activity. Our findings reveal that changes in dFPN oscillatory activity correspond to unique behavioral states. Lastly, we showed that the stability of dFPN theta phase synchrony predicts more stable attentional performance. Our study underscores the potential of theta-connectivity modulation to enhance attentional performance and provides new insights into the neural and behavioral strategies that support SA under high demands.

4. Methods

4.1. Experimental procedures

4.1.1. Animals

Three spayed female ferrets (*Mustela putorius furo*), 16–19 weeks old and weighing 0.7–1 kg, were purchased from Marshal BioResources, North Rose, NY. Animals were group housed in a 12 hr light/12 hr dark cycle and all procedures were done in compliance with the Institutional Animal Care and Use Committee of the University of North Carolina at Chapel Hill and the United States Department of Agriculture (USDA Animal Welfare).

Included in the analysis of behavioral data are 26 short-delay sessions (Animal A = 10, Animal B = 8, Animal C = 8) and 34 long-delay sessions (Animal A = 12, Animal B = 11, Animal C = 11). For analysis of brain data, 5 sessions were excluded based on errors during recording, resulting in 23 short-delay sessions (Animal A = 8, Animal B = 8, Animal C = 7) and 32 long-delay sessions (Animal A = 12, Animal B = 9, Animal C = 11).

4.1.2. Behavioral training

Detailed procedure in (Sellers et al., 2016; Huang et al., 2024; Yu et al., 2018).

The 5-CSRTT is a self-paced, freely moving visual attention task that requires animals to wait a variable amount of time to respond to a visual stimulus and retrieve water reward. In brief, each trial of the 5-CSRTT includes the following steps: trial initiation, variable waiting period, presentation of visual stimulus and intertrial interval dependent on animal response. Training followed procedures reported in previous papers with waiting time randomized between 4, 5, and 6 seconds. After animals reached baseline criterion ($\geq 80\%$ accuracy), the two task conditions, short or long-delay period, were introduced. The order of session type was randomized, and each session included 80 trials with randomized order of waiting time. The distribution of wait times for long-delay sessions are: 85 % (68) of trials are 9 s, 10 % (8) 7 s, and 5 % (4) 4 s. For short-delay sessions the trial proportions are identical, except 85 % of trials are 4 s and 5 % are 9 s. Animals were trained on short and long-delay sessions until accuracy was on average $> 70\%$ and $> 60\%$, respectively. Animals were on a 5 day on/2 days off water deprivation schedule and trained twice daily during deprivation

(average session duration 20 min). Supplemental water was provided at the end of every training day to ensure each animal maintained an average water intake of 60 mL/kg/day. Animal health was assessed daily via weight monitoring and observation researchers reported to university veterinarians if an animal's weight reduced more than 15 % in one week or abnormal behavior caused concern.

4.1.3. Multielectrode array implantation surgery

After behavioral training, animals underwent surgery to implant multielectrode arrays in frontal (PMC) and parietal (PPC) cortical nodes of the dorsal frontoparietal network, previously determined (Sellers et al., 2016). An injection of a ketamine/xylazine mix (30 mg/kg of ketamine, 1–2 mg/kg of xylazine, intramuscular) was administered to induce anesthesia, volume proportional to animal weight. After establishing a stable plane of anesthesia (no-toe pinch response), the following procedures were performed: top of head, chest and feet were shaved and cleaned with ethanol, EKG pads applied, preoperative medication injected (0.2 mg/kg meloxicam, subcutaneous), eye lubricant applied (Paralube), intubation and transfer to stereotaxic surgery setup and ventilator. Aseptic conditions were initiated (details in (Sellers et al., 2013; 2015; Huang et al., 2024)) and scalp was cleaned with alternating betadine and alcohol wipes. Isoflurane (1–2 %) in 100 % oxygen was used to maintain anesthetic depth throughout surgery. Depth of anesthesia was continuously monitored via recordings of end tidal CO₂, electrocardiogram, partial oxygen saturation and rectal temperature. Saline was injected every hour (10 mL/kg 1st hr, 5 mL/kg 2nd hr, 2.5 mL/kg 3rd-final hr) subcutaneously to keep the animal hydrated and support recovery.

Two craniotomies were performed over the PMC and PPC on the left hemisphere, dura and pia were subsequently removed. Anatomical targeting was planned based on atlas coordinates in reference to occipital crest (Radtke-Schuller, 2018) and are as follows: PMC; −26.1 mm AP, 4 mm ML, −2 mm DV and PPC; −13 mm AP, 3.5 mm ML, −1 mm DV. A 16-channel optrode (an optical fiber in the middle of two concentric circles of electrodes; platinum/iridium electrode, 125 μm diameter, 5 mm length, 250 μm spacing; fiber optic 4.5 mm long, 200 μm core outer diameter, 0.48 numerical aperture; Microprobes for life science, Gaithersburg, MD) was implanted in the PMC. An optrode was chosen because these animals were also a part of an optogenetic experiment, whose findings are not reported here. A second electrode array (2 × 8 tungsten electrodes, 35 μm diameter, 5 mm length, 200 μm spacing; local reference 500 μm shorter, Innovative Neurophysiology Durham, NC) was implanted in the PPC. Electrophysiology was monitored during array implantation and used to determine final implant depth based on when spiking activity was observed on about half the channels (slant of cortex prevents all channels from recording in spike-rich layers). Each electrode included a silver wire for grounding that was wrapped around grounding bone screws partially drilled into the skull. To help secure the cap to the skull, additional bone screws were partially drilled into the skull. Cranial windows were closed with silicon (Kwik-Cast™ Silicone Elastomer, World Precision Instruments) and electrodes were stabilized with dental cement. Excess loose skin was sutured at the front and back of the headcap. The animal was closed monitored for the following week; pain medication (0.2 mg/kg meloxicam, subcutaneous) 3 days, oral antibiotic (12.5–13 mg/kg) twice daily for 7 days. During this post-operative time the animals were given *ad libitum* water access. Regular headcap cleaning and monitoring was performed and reported in a log twice weekly until end of experiment.

4.1.4. In vivo electrophysiology recordings

Following one week of recovery from surgery, animals resumed behavioral training until they regained pre-surgery levels of performance (about one week). During task performance, electrophysiological data was continuously acquired with 30 kHz sampling rate and bandwidth 0.1–5 kHz (RHD2132 amplifier boards connected to RHD2000 USB Interface Boards, Intan Technologies, Los Angeles, CA). To enable

unrestricted motion during behavior, a commutator (AC32, Tucker-Davis Technologies, Alachua, FL) with custom built adapters was used. Task features (i.e., initiation, screen touch) and electrophysiology were simultaneously recorded by digital input to ensure neurophysiology and behavior were properly aligned. The two session conditions (short or long-delay) were randomized to prevent a confound of training effect.

4.1.5. Histology and verification of electrode locations

Animals were deeply anesthetized at the end of the experiment by injecting an overdose of ketamine/xylazine intramuscularly and then transcardially perfused (4 % paraformaldehyde in phosphate-buffered saline). Following perfusion, the brain was removed from the skull and left overnight in 4 % paraformaldehyde solution before transferring to a cryoprotectant solution of 30 % phosphate-buffered sucrose. The brain was left in cryoprotection until the brain sank (~ 7 days). The brain was then flash frozen and sectioned in the standard frontal plane of the ferret atlas (Radtke-Schuller, 2018) into 6 parallel series of 50 thick sections on a freezing microtome. At least one set of serial sections was used for a cell stain (Nissl). A bright-field slide scanner at 10x magnification (Aperio VERSA) was used to image Nissl sections. Subsequent analysis compared the stained sections with ferret atlas plates to determine the recording location based on cortical tissue damage and characteristic glia cell accumulation.

4.1.6. Data analysis

Data analysis was carried out offline with custom MATLAB R2022a (MathWorks) scripts.

4.1.6.1. Preprocessing. Raw electrophysiological data was low-band pass filtered (MATLAB filtfilt, 2nd order Butterworth filter with 300 Hz cutoff) and then down sampled (30 kHz to 1 kHz) to obtain local field potential (LFPs). Artifacts (from excessive movement, line noise or damaged equipment) were removed with Artifact Subspace Reconstruction (ASR) method in EEGLAB. LFP data was then aligned to behavior using event time stamps recorded during the 5-CSRTT. All analysis is aligned to initiation of correct trials of principle waiting period for each session (-10 to 1 s relative to 9 s trials in long-delay sessions; -5 to 1 s relative to 4 s trials in short-delay sessions).

Multi- and single-unit spiking activity was obtained from recorded extracellular potentials isolated by alternatively band-pass filtering the raw electrophysiological data (300–5000 Hz). A threshold (-3.5 standard deviations below mean) was then applied to the filtered data. To isolate single-units, template matching in Kilosort and Kilosort2 (Pachitariu et al., 2016) was performed followed by manual curation in Phy (visual inspection of waveform and autocorrelogram).

4.1.6.2. Spectral analysis. Time-frequency analysis of LFPs was achieved with wavelet convolution. The Morlet wavelet can be defined as a complex exponential modulated by a Gaussian factor:

$$\text{wav}(t, f_0) = A \cdot \exp\left(-\frac{t^2}{2\sigma_t^2}\right) \cdot \exp(-2i\pi f_0 t)$$

where f_0 denotes the wavelet's central frequency (with 150 values logarithmically distributed between 2 and 128 Hz), while constant $A = (\sigma_t \sqrt{\pi})^{-1/2}$ ensures wavelet energy is normalized to 1. Standard deviation of the time-domain ($\sigma_t = 2\pi\sigma_f$) is expressed as a function of the standard deviation of the frequency-domain (σ_f). Spectral data was then averaged across channels, trials, and session condition per animal. The aperiodic component of the signal was isolated from the averaged data with foof toolbox in MATLAB and then removed from each session individually (Leroy et al. 2022).

4.1.6.3. Linear regression and change point detection. The fitlm function

in MATLAB was used to fit a linear regression to each isolated frequency band (predictor) throughout time (response variable, 100 Hz sampling rate) of the delay period. This function uses the least squares method to estimate the coefficients of the linear model and minimize the sum of squared residuals to find the best-fitting line,

$$\text{slope} = \frac{n \sum xy - \sum x \sum y}{n \sum x^2 - (\sum x)^2}$$

where x is the predictor (i.e., time from trial initiation to visual stimulus onset), y is response variable (i.e., frequency-specific spectral power, functional connectivity) and n represent number of samples. Reported slope value came from the model coefficient estimate. Change point detection was carried out to find abrupt changes in the isolated power spectral density of each frequency band of interest. A MATLAB function (`findchangepts` in Matlab Signal Processing Toolbox) was used to return the index of the response variable where the predictor changed most significantly in mean or mean and slope. Residuals from this function represent the differences between consecutive data points in the time series and are interpreted as a measure of change or deviation from overall pattern in the data.

4.1.6.4. Spectral contrast. Two spectral contrasts were of experimental interest: In test one, we contrasted (A) first 4 s of waiting period in long-delay 9 s trials and (B) full waiting period of short-delay 4 s trials. In test two, (A) was contrasted with (C) last 4 s of waiting period in long-delay 9 s trials. We applied cluster-based nonparametric statistical testing following previous procedures (Huang et al., 2024). In this method, multiple comparisons across time-frequency clusters is appropriately controlled for.

To begin, cluster size (minimum 30) of observed data was computed for each condition and region. Next, baseline was established by randomly swapping half of the condition labels (i.e., swapping labels A and B or A and C) and calculating the contrast between newly swapped condition labels. This provided a reference where differences between conditions are expected to be eliminated. Condition labels were then randomly permuted 1000 times to create the null distribution of cluster sizes under the assumption that there is no difference between conditions. From this distributions, the 5th and 95th percentile values were selected as critical size values. Clusters in the observed data with sizes more extreme than identified critical values are considered statistically significant with a significance threshold of $\alpha = 0.05$. Finally, the results are visualized by plotting contours on high-resolution difference plots for interpretation.

4.1.6.5. Behavioral Motion Tracking. Ferret head position during 5-CSRTT performance was analyzed by tracking video recordings of animal behavior with DeepLabCut (version 2.3.9), an open-source, deep learning-based toolbox for markerless motion tracking from videos (Mathis et al., 2018; Nath et al., 2019). We trained a deep neural network to precisely track the head position of ferrets during the 5-CSRTT. Three behavioral videos were used to train the network (Animal A: short-delay (6 min, 11 s), long-delay (18 min, 55 s), Animal B: long-delay (14 min, 47 s)), where the final training set included 600 frames. A ResNet50-based neural network was then trained with DeepLabCut default parameters for 300,000 iterations using a high-performance computer with a 12th-generation Intel i9 CPU (16 cores) and an NVIDIA GeForce RTX 3080 GPU. The trained network evaluated 25 videos of long-delay task performance across three animals (Animal A = 8, Animal B = 7, Animal C = 10). A decoded time series was generated in DeepLabCut and was subsequently low band-pass filtered (Python `scipy.signal`, 4th order Butterworth filter, 0.14 Hz cutoff) and visually inspected. Decoded time series data was isolated between initiation and visual stimulus onset for all correct trials of principle delay duration for long-delay sessions (9 s). Across animals, 802 trials were analyzed (Animal A = 247, Animal B = 271 and Animal C = 285).

Velocity was calculated iteratively at each time step (60 frames per second) by subtracting the current and preceding head position and dividing by time step duration. Final velocity values represent an average across correct trials. Two-dimensional histograms were generated from the time series data of animal head position at 3 s, 5 s and 8 s after trial initiation. Data is normalized to total trial number to account for variation across animals. Spatial representation of head position was converted from pixels to centimeters (cm) by multiplying pixel position by the ratio between the physical length (61.20 cm) and width (50.60 cm) of the behavior chamber and the height (1920 pixels) and width (1080 pixels) of video recording for each time step. Where final bin size is 0.55 cm² (100 bins on x-axis, 56 bins on y-axis).

4.1.6.6. Functional and effective connectivity. Phase locking value (PLV) was computed between PMC and PPC LFP signals to assess functional phase-connectivity of the network during the waiting period of each 5-CSRTT condition. For each possible channel pair between PMC and PPC, the phase locking value (PLV) was determined, resulting in a value between 0 and 1, calculated as:

$$\text{PLV}_{mn}(t, f_0) = \left| \frac{1}{K} \sum_{k=1}^K e^{i(\varphi_k^m(t, f_0) - \varphi_k^n(t, f_0))} \right|$$

For every trial (K), PLV between PMC (m) and PPC (n), was calculated based on instantaneous phase of a channel from each region ($\varphi_k^m(t, f_0)$ and $\varphi_k^n(t, f_0)$) for frequency f_0 via Morlet wavelet transform. PLV for each pair of valid channels were averaged across session for each condition. Specifically, power of theta-band PLV (4–6.5 Hz) was isolated for condition contrast and significance was determined by linear mixed modeling.

Effective connectivity was analyzed via pairwise spectral Granger Causality using the MVGC (Multivariate Granger Causality) MATLAB toolbox (Barnett and Seth, 2014; Huang et al., 2024). The LFP signal from each analyzed region was low pass filtered (2nd order Butterworth), resampled (200 Hz) and aligned to trial initiation event time stamps. Via a sliding window approach, an autoregressive model (AR, order 20) was fitted to the data to estimate the autocovariance sequence. Granger Causality was then computed based on autocovariance and interpolated to frequencies of interest (2–128 Hz). Theta-band GC (4–6.5 Hz) was isolated for top-down (PMC → PPC) and bottom-up (PPC → PMC) data, outliers were removed (> 3 standard deviations from median) and mixed modeling was carried out to demonstrate statistically if theta-band PLV a top-down or bottom-up network signature.

4.1.6.7. Brain-behavior correlation. We used linear mixed modeling and spearman correlation in R to observe the relationship between brain signal and behavioral performance. Power of theta-band PLV (4–6.5 Hz) was isolated for the waiting period and averaged across trials for every session. Robust linear regression was performed in MATLAB (`fitlm` function), with the slope describing the change in theta-band PLV over the duration of the waiting period. To correlate with change in theta-PLV, the coefficient of variation (CV) was calculated for reaction time within session ((sd/mn) * 100). The ‘`romr.fnc`’ function from the ‘`LMERConvenienceFunctions`’ was used to trim the top and bottom 3 % of residuals from the data. Slope of theta-PLV was centered and scaled within factor level for condition. Our mixed model demonstrated that inclusion of slope of theta-PLV as a predictor improved model fit for the CV of reaction time ($p < 0.001$). Further, spearman correlation test returned a near-significant negative correlation ($r = -0.327$, $p = 0.068$).

4.1.6.8. Accuracy. We included two measurements to reflect behavioral performance within each session: Overall Accuracy and Post-Stimulus Accuracy. The Overall Accuracy calculation includes all trial outcome possibilities in the denominator, as reported in the original 5-CSRTT (Sellers et al., 2016; Huang et al., 2024). In contrast, Post-Stimulus Accuracy considers only trials where animals had the opportunity to

detect the stimulus, excluding premature responses from the denominator. This second measurement was included to demonstrate that differences in accuracy between task conditions are not necessarily due to the animals' ability to detect stimuli, but rather their ability to inhibit premature responses.

$$\text{Overall Accuracy} = \frac{\text{Correct}}{\text{Correct} + \text{Premature} + \text{Omission} + \text{Incorrect}}$$

$$\text{Post-Stimulus Accuracy} = \frac{\text{Correct}}{\text{Correct} + \text{Omission} + \text{Incorrect}}$$

4.1.6.9. Statistical analysis. Linear mixed modeling was used in R studio to assess the relationship between session condition (short vs long-delay) and behavioral outcome while controlling for random effect of individual animal differences "Measure ~ Condition + (1 + Day | AnimalID)" where significance level is $\alpha = 0.05$. For Granger Causality calculation, Condition was either 'bottom-up' or 'top-down' rather than 'short-delay' or 'long-delay'. Dependent variables were scaled, and the Holm-Bonferroni method was used to correct p-values. The 'romr.fnc' function from the 'LMERConvenienceFunctions' was used to trim the top and bottom 3 % of residuals from the data.

4.1.6.10. Frequencies of interest. Frequency bands of interest in our statistical testing and data visualization are as follows: theta 4–7 Hz, alpha 16–19 Hz, gamma 56–59 Hz.

CRediT authorship contribution statement

Jared Reiling: Writing – review & editing, Visualization, Formal analysis. **Huang Angel:** Writing – review & editing, Resources, Methodology. **Mengsen Zhang:** Writing – review & editing, Supervision. **Jimin Park:** Writing – review & editing, Validation. **Joseph Hopfinger:** Writing – review & editing, Methodology. **Susanne Radtke-Schuller:** Writing – review & editing, Methodology. **Flavio Frohlich:** Writing – review & editing, Supervision, Methodology, Funding acquisition, Conceptualization. **Agnieszka Zuberer:** Writing – review & editing. **Grace Ross:** Writing – original draft, Visualization, Methodology, Investigation, Formal analysis, Conceptualization.

Code and data availability

TBD.

Declaration of Generative AI and AI-assisted technologies in the writing process

During the preparation of this work generative AI (ChatGPT 3.5) was used for light editing and language improvement. After using this tool, a human author reviewed and edited the content as needed and takes full responsibility for the content of the publication.

Declaration of Competing Interest

The authors declare that they have no known competing financial interests or personal relationships that could have appeared to influence the work reported in this paper.

Acknowledgements

The authors would like to thank Peyton Siekierski and Abdulaziz Norbekov for assistance in animal surgeries and data collection. We gratefully recognize our funding sources: National Institutes of Health Grant R01MH124387 (F.F.) and National Institutes of Health R01MH122477 (F.F.).

Appendix A. Supporting information

Supplementary data associated with this article can be found in the online version at doi:10.1016/j.pneurobio.2025.102777.

Data Availability

Data will be made available on request.

References

- Alagapan, Sankaraleengam, Schmidt, Stephen L., Lefebvre, Jérémie, Hadar, Eldad, Shin, Hae Won, Fröhlich, Flavio, 2016. Modulation of cortical oscillations by low-frequency direct cortical stimulation is state-dependent. PLoS Biol. 14 (3), e1002424. <https://doi.org/10.1371/journal.pbio.1002424>.
- Barkley, Russell A., 1997. Behavioral inhibition, sustained attention, and executive functions: constructing a unifying theory of ADHD. Psychol. Bull. 121 (1), 65–94. <https://doi.org/10.1037/0033-2909.121.1.65>.
- Barnes, Samuel A., Young, Jared W., Neill, Jo.C., 2012. D₁ receptor activation improves vigilance in rats as measured by the 5-choice continuous performance test. Psychopharmacology 220 (1), 129–141. <https://doi.org/10.1007/s00213-011-2460-8>.
- Barnett, Lionel, Seth, Anil K., 2014. The MVGC multivariate granger causality toolbox: a new approach to granger-causal inference. J. Neurosci. Methods 223 (February), 50–68. <https://doi.org/10.1016/j.jneumeth.2013.10.018>.
- Baumeister, Roy F., Bratslavsky, Ellen, Muraven, Mark, Tice, Dianne M., 1998. Ego depletion: is the active self a limited resource? J. Personal. Soc. Psychol. 74 (5), 1252–1265. <https://doi.org/10.1037/0022-3514.74.5.1252>.
- Bora, Emre, Vahip, Simavi, Akdeniz, Fisun, 2006. Sustained attention deficits in manic and euthymic patients with bipolar disorder. Prog. Neuro-Psychopharmacol. Biol. Psychiatry 30 (6), 1097–1102. <https://doi.org/10.1016/j.pnpbp.2006.04.016>.
- Carli, M., Robbins, T.W., Evenden, J.L., Everitt, B.J., 1983. Effects of lesions to ascending noradrenergic neurones on performance of a 5-choice serial reaction task in rats; implications for theories of dorsal noradrenergic bundle function based on selective attention and arousal. Behavioural Brain Research 9 (3), 361–380. [https://doi.org/10.1016/0166-4328\(83\)90138-9](https://doi.org/10.1016/0166-4328(83)90138-9).
- Cavanagh, James F., Frank, Michael J., 2014. Frontal theta as a mechanism for cognitive control. Trends Cogn. Sci. 18 (8), 414–421. <https://doi.org/10.1016/j.tics.2014.04.012>.
- Cavanagh, James F., Gregg, David, Light, Gregory A., Olguin, Sarah L., Sharp, Richard F., Bismark, Andrew W., Bhakta, Savita G., Swerdlow, Neal R., Brigman, Jonathan L., Young, Jared W., 2021. Electrophysiological biomarkers of behavioral dimensions from cross-species paradigms. Transl. Psychiatry 11 (1), 482. <https://doi.org/10.1038/s41398-021-01562-w>.
- Chen, Liu, Du, Bang, Li, Ke, Li, Kaiyun, Hou, TingTing, Jia, Fanlu, Li Li, 2024. The effect of tDCS on inhibitory control and its transfer effect on sustained attention in children with autism spectrum disorder: an fNIRS study. Brain Stimul. 17 (3), 594–606. <https://doi.org/10.1016/j.brs.2024.04.019>.
- Clayton, Michael S., Yeung, Nick, Cohen Kadosh, Roi, 2015. The roles of cortical oscillations in sustained attention. Trends Cogn. Sci. 19 (4), 188–195. <https://doi.org/10.1016/j.tics.2015.02.004>.
- deBettencourt, Megan T., Cohen, Jonathan D., Lee, Ray F., Norman, Kenneth A., Turk-Browne, Nicholas B., 2015. Closed-loop training of attention with real-time brain imaging. Nat. Neurosci. 18 (3), 470–475. <https://doi.org/10.1038/nn.3940>.
- Demirayak, Pınar, Küyi, İlayda, İşbitiren, Yağmur Özbeş, Yener, Görsev, 2023. Cognitive load associates prolonged P300 latency during target stimulus processing in individuals with mild cognitive impairment. Sci. Rep. 13 (1), 15956. <https://doi.org/10.1038/s41598-023-43132-8>.
- Dosenbach, Nico U.F., Fair, Damien A., Miezin, Francis M., Cohen, Alexander L., Wenger, Kristin K., Dosenbach, Ronny A.T., Fox, Michael D., et al., 2007. Distinct brain networks for adaptive and stable task control in humans. Proc. Natl. Acad. Sci. 104 (26), 11073–11078. <https://doi.org/10.1073/pnas.0704320104>.
- Drummond, Sean P.A., Bischoff-Grethe, Amanda, Dinges, David F., Ayalon, Liat, Mednick, Sara C., Meloy, M.J., 2005. The neural basis of the psychomotor vigilance task. Sleep 28 (9), 1059–1068.
- Durmer, Jeffrey S., Dinges, David F., 2005. Neurocognitive consequences of sleep deprivation. Semin. Neurol. 25 (01), 117–129. <https://doi.org/10.1055/s-2005-867080>.
- Eisma, Jarrod, Rawls, Eric, Long, Stephanie, Mach, Russell, Lamm, Connie, 2021. Frontal midline theta differentiates separate cognitive control strategies while still generalizing the need for cognitive control. Sci. Rep. 11 (1), 14641. <https://doi.org/10.1038/s41598-021-94162-z>.
- Epstein, Jeffery N., Langberg, Joshua M., Rosen, Paul J., Graham, Amanda, Narad, Megan E., Antonini, Tanya N., Brinkman, William B., Froehlich, Tanya, Simon, John O., Altaye, Mekhib, 2011. Evidence for higher reaction time variability for children with ADHD on a range of cognitive tasks including reward and event rate manipulations. Neuropsychology 25 (4), 427–441. <https://doi.org/10.1037/a0022155>.
- Esterman, Michael, Noonan, Sarah K., Rosenberg, Monica, Degutis, Joseph, 2013. In the zone or zoning out? Tracking behavioral and neural fluctuations during sustained attention. Cereb. Cortex (N. Y., N. Y.: 1991) 23 (11), 2712–2723. <https://doi.org/10.1093/cercor/bhs261>.

- Esterman, Michael, Rothlein, David, 2019. Models of sustained attention. *Curr. Opin. Psychol.* 29 (October), 174–180. <https://doi.org/10.1016/j.copsyc.2019.03.005>.
- Fang, Qi, Frohlich, Flavio, 2023. Dissection of neuronal circuits underlying sustained attention with the five-choice serial reaction time task. *Neurosci. Biobehav. Rev.* 152 (September), 105306. <https://doi.org/10.1016/j.neubiorev.2023.105306>.
- Gbadeyan, Oyetunde, Teng, James, Prakash, Ruchika Shaurya, 2022. Predicting response time variability from task and resting-state functional connectivity in the aging brain. *NeuroImage* 250 (April), 118890. <https://doi.org/10.1016/j.neuroimage.2022.118890>.
- Goswami, U., Sharma, A., Varma, A., Gulrajani, C., Ferrier, I.N., Young, A.H., Gallagher, P., Thompson, J.M., Moore, P.B., 2009. The neurocognitive performance of drug-free and medicated euthymic bipolar patients do not differ. *Acta Psychiatr. Scand.* 120 (6), 456–463. <https://doi.org/10.1111/j.1600-0447.2009.01390.x>.
- Helfrich, Randolph F., Fiebelkorn, Ian C., Szczepanski, Sara M., Lin, Jack J., Parviz, Josef, Knight, Robert T., Kastner, Sabine, 2018. Neural mechanisms of sustained attention are rhythmic. *Neuron* 99 (4), 854–865.e5. <https://doi.org/10.1016/j.neuron.2018.07.032>.
- Huang, Wei A., Stitt, Iain M., Negahbani, Ehsan, Passey, D.J., Ahn, Sangtae, Davey, Marshall, Dannhauer, Moritz, et al., 2021. Transcranial alternating current stimulation entrains alpha oscillations by preferential phase synchronization of fast-spiking cortical neurons to stimulation waveform. *Nat. Commun.* 12 (1), 3151. <https://doi.org/10.1038/s41467-021-23021-2>.
- Huang, Wei A., Zhou, Zhe C., Stitt, Iain M., Ramasamy, Nivetha S., Radtke-Schuller, Susanne, Frohlich, Flavio, 2024. Causal oscillations in the visual thalamo-cortical network in sustained attention in ferrets. *Curr. Biol.* 34 (4), 727–739.e5. <https://doi.org/10.1016/j.cub.2023.12.067>.
- Jensen, Ole, Mazaheri, Ali, 2010. Shaping functional architecture by oscillatory alpha activity: gating by inhibition. *Front. Hum. Neurosci.* 4, 186. <https://doi.org/10.3389/fnhum.2010.00018>.
- Johnson, Elizabeth L., Lin, Jack J., King-Stephens, David, Weber, Peter B., Laxer, Kenneth D., Saez, Ignacio, Grgis, Fady, D'Esposito, Mark, Knight, Robert T., Badre, David, 2023. A rapid theta network mechanism for flexible information encoding. *Nat. Commun.* 14 (1), 2872. <https://doi.org/10.1038/s41467-023-38574-7>.
- Lavie, Nilli, 1995. Perceptual load as a necessary condition for selective attention. *J. Exp. Psychol.: Hum. Percept. Perform.* 21 (3), 451–468. <https://doi.org/10.1037/0096-1523.21.3.451>.
- Lavie, Nilli, De Fockert, Jan, 2005. The role of working memory in attentional capture. *Psychon. Bull. Rev.* 12 (4), 669–674. <https://doi.org/10.3758/BF03196756>.
- Lavie, Nilli, Polly, Dalton, 2014. In: Anna, C. (Kia) Nobre, Kastner, Sabine (Eds.), Load Theory of Attention and Cognitive Control, 1. Oxford University Press. <https://doi.org/10.1093/oxfordhb/9780199675111.013.003>.
- Lavie, Nilli, Tsai, Yehoshua, 1994. Perceptual load as a major determinant of the locus of selection in visual attention. *Percept. Psychophys.* 56 (2), 183–197. <https://doi.org/10.3758/BF03213897>.
- Leroy, Sophie, Major, Sebastian, Bublitz, Viktor, Dreier, Jens P., Koch, Susanne, 2022. Unveiling age-independent spectral markers of propofol-induced loss of consciousness by decomposing the electroencephalographic spectrum into its periodic and aperiodic components. *Front. Aging Neurosci.* 14, 1076393. <https://doi.org/10.3389/fnagi.2022.1076393>.
- Li, Yujuan, Ji, Luyan, 2024. Ensemble coding of multiple facial expressions is not affected by attentional load. *BMC Psychol.* 12 (1), 102. <https://doi.org/10.1186/s40359-024-01598-9>.
- Lundqvist, Mikael, Bastos, André M., Miller, Earl K., 2020. Preservation and changes in oscillatory dynamics across the cortical hierarchy. *J. Cogn. Neurosci.* 32 (10), 2024–2035. https://doi.org/10.1162/jocn_a_01600.
- Lustenberger, Caroline, Boyle, Michael R., Alagapan, SankaraIengam, Mellin, Julianne M., Vaughn, Bradley V., Fröhlich, Flavio, 2016. Feedback-controlled transcranial alternating current stimulation reveals a functional role of sleep spindles in motor memory consolidation. *Curr. Biol.* 26 (16), 2127–2136. <https://doi.org/10.1016/j.cub.2016.06.044>.
- MacDonald, Stuart W.S., Li, Shu-Chen, Bäckman, Lars, 2009. Neural underpinnings of within-person variability in cognitive functioning. *Psychol. Aging* 24 (4), 792–808. <https://doi.org/10.1037/a0017798>.
- MacDonald, Stuart W.S., Nyberg, Lars, Bäckman, Lars, 2006. Intra-individual variability in behavior: links to brain structure, neurotransmission and neuronal activity. *Trends Neurosci.* 29 (8), 474–480. <https://doi.org/10.1016/j.tins.2006.06.011>.
- Marek, Scott, Dosenbach, Nico U.F., 2018. The frontoparietal network: function, electrophysiology, and importance of individual precision mapping. *Dialog. Clin. Neurosci.* 20 (2), 133–140. <https://doi.org/10.31887/DCNS.2018.20.2/smarek>.
- Mathis, Alexander, Mamidanna, Pranav, Cury, Kevin M., Abe, Taiga, Murthy, Venkatesh N., Mathis, Mackenzie Weygandt, Bethge, Matthias, 2018. DeepLabCut: markerless pose estimation of user-defined body parts with deep learning. *Nat. Neurosci.* 21 (9), 1281–1289. <https://doi.org/10.1038/s41593-018-0209-y>.
- McFerren, Amher, Riddle, Justin, Walker, Christopher, Buse, John B., Frohlich, Flavio, 2021. Causal role of frontal-midline theta in cognitive effort: a pilot study. *J. Neurophysiol.* 126 (4), 1221–1233. <https://doi.org/10.1152/jn.00068.2021>.
- McGaughy, J., Sarter, M., 1995. Behavioral vigilance in rats: task validation and effects of age, amphetamine, and benzodiazepine receptor ligands. *Psychopharmacology* 117 (3), 340–357. <https://doi.org/10.1007/BF02246109>.
- Minami, Sorato, Watanabe, Ken, Saijo, Naoki, Kashino, Makio, 2023. Neural oscillation amplitude in the frontal cortex predicts esport results. *iScience* 26 (6), 106845. <https://doi.org/10.1016/j.isci.2023.106845>.
- Murphy, Gillian, Groeger, John A., Greene, Ciara M., 2016. Twenty years of load theory—where are we now, and where should we go next? *Psychon. Bull. Rev.* 23 (5), 1316–1340. <https://doi.org/10.3758/s13423-015-0982-5>.
- Nath, Tammay, Mathis, Alexander, Chen, An. Chi, Patel, Amir, Bethge, Matthias, Mathis, Mackenzie Weygandt, 2019. Using DeepLabCut for 3D markerless pose estimation across species and behaviors. *Nat. Protoc.* 14 (7), 2152–2176. <https://doi.org/10.1038/s41596-019-0176-0>.
- Nielsen, B., Hyldig, T., Bidstrup, F., González-Alonso, J., Christoffersen, G.R., 2001. Brain activity and fatigue during prolonged exercise in the heat. *Pflug. Arch.: Eur. J. Physiol.* 442 (1), 41–48. <https://doi.org/10.1007/s004240100515>.
- Nobre, Anna C. (Kia), Sabine Kastner, 2014. In: Anna, C. (Kia) Nobre, Kastner, Sabine (Eds.), Attention, 1. Oxford University Press. <https://doi.org/10.1093/oxfordhb/9780199675111.013.040>.
- Nuechterlein, Keith H., Green, Michael F., Calkins, Monica E., Greenwood, Tiffany A., Gur, Raquel E., Gur, Ruben C., Lazzeroni, Laura C., et al., 2015. Attention/vigilance in schizophrenia: performance results from a large multi-site study of the consortium on the genetics of schizophrenia (COGS). *Schizophr. Res.* 163 (1–3), 38–46. <https://doi.org/10.1016/j.schres.2015.01.017>.
- Pachitariu, M., Steinmetz, N.A., Kadir, S.N., Carandini, M., Harris, K.D., 2016. Advances in neural information processing systems. *Adv. Inf. Process. Syst.* 4448–4456.
- Pagliaccio, David, Wiggins, Jillian Lee, Adleman, Nancy E., Harkins, Elizabeth, Curhan, Alexa, Towbin, Kenneth E., Brozman, Melissa A., Pine, Daniel S., Leibenluft, Ellen, 2017. Behavioral and neural sustained attention deficits in bipolar disorder and familial risk of bipolar disorder. *Biol. Psychiatry* 82 (9), 669–678. <https://doi.org/10.1016/j.biopsych.2016.09.006>.
- Qu, Hongyu, Zhao, Shuo, Li, Zimo, Wu, Jinglong, Murai, Toshiya, Li, Qi, Wu, Yan, Zhang, Zhilin, 2024. Investigating the impact of schizophrenia traits on attention: the role of the theta band in a modified posner cueing paradigm. *Cereb. Cortex (N. Y., N. Y.): 1991* 34 (7), bhae274. <https://doi.org/10.1093/cercor/bhae274>.
- Radtke-Schuller, Susanne, 2018. Cyto- and Myeloarchitectural Brain Atlas of the Ferret (*Mustela putorius*) in MRI Aided Stereotaxic Coordinates. 1st ed. Springer Cham..
- Reck, Sarah G., Hund, Alycia M., 2011. Sustained attention and age predict inhibitory control during early childhood. *J. Exp. Child Psychol.* 108 (3), 504–512. <https://doi.org/10.1016/j.jecp.2010.07.010>.
- Riccio, C.A., Waldrop, J.J., Reynolds, C.R., Lowe, P., 2001. Effects of stimulants on the continuous performance test (CPT): implications for CPT use and interpretation. *J. Neuropsychiatry Clin. Neurosci.* 13 (3), 326–335. <https://doi.org/10.1176/jnp.13.3.326>.
- Riddle, Justin, McPherson, Trevor, Sheikh, Atif, Shin, Haewon, Hadar, Eldad, Frohlich, Flavio, 2024. Internal representations are prioritized by frontoparietal theta connectivity and suppressed by alpha oscillation dynamics: evidence from concurrent transcranial magnetic stimulation EEG and invasive EEG. *J. Neurosci.: Off. J. Soc. Neurosci.* 44 (15), e1381232024. <https://doi.org/10.1523/JNEUROSCI.1381-23.2024>.
- Riddle, Justin, Scimeca, Jason M., Cellier, Dillan, Dhanani, Sofia, D'Esposito, Mark, 2020. Causal evidence for a role of theta and alpha oscillations in the control of working memory. *Curr. Biol.* 30 (9), 1748–1754.e4. <https://doi.org/10.1016/j.cub.2020.02.065>.
- Rosenberg, Monica D., Finn, Emily S., Scheinost, Dustin, Papademetris, Xenophon, Shen, Xilin, Constable, R.Todd, Chun, Marvin M., 2016. A neuromarker of sustained attention from whole-brain functional connectivity. *Nat. Neurosci.* 19 (1), 165–171. <https://doi.org/10.1038/nn.4179>.
- Ross, Grace, Radtke-Schuller, Susanne, Frohlich, Flavio, 2024. Ferret as a model system for studying the anatomy and function of the prefrontal cortex: a systematic review. *Neurosci. Biobehav. Rev.* 162 (July), 105701. <https://doi.org/10.1016/j.neubiorev.2024.105701>.
- Sarter, M., Givens, B., Bruno, J.P., 2001. The cognitive neuroscience of sustained attention: where top-down meets bottom-up. *N. Res. Rev.* 35 (2), 146–160. [https://doi.org/10.1016/s0165-0173\(01\)00044-3](https://doi.org/10.1016/s0165-0173(01)00044-3).
- Schmidt, Stephen L., Iyengar, Apoorva K., Foulser, A., Alban, Boyle, Michael R., Fröhlich, Flavio, 2014. Endogenous cortical oscillations constrain neuromodulation by weak electric fields. *Brain Stimul.* 7 (6), 878–889. <https://doi.org/10.1016/j.brs.2014.07.033>.
- Seeburger, Dolly T., Xu, Nan, Ma, Marcus, Larson, Sam, Godwin, Christine, Keilholz, Sheila D., Schumacher, Eric H., 2024. Time-varying functional connectivity predicts fluctuations in sustained attention in a serial tapping task. *Cogn., Affect., Behav. Neurosci.* 24 (1), 111–125. <https://doi.org/10.3758/s13415-024-01156-1>.
- Sellers, Kristin K., Bennett, Davis V., Hutt, Axel, Fröhlich, Flavio, 2013. Anesthesia differentially modulates spontaneous network dynamics by cortical area and layer. *J. Neurophysiol.* 110 (12), 2739–2751. <https://doi.org/10.1152/jn.00404.2013>.
- Sellers, Kristin K., Mellin, Julianne M., Lustenberger, Caroline M., Boyle, Michael R., Lee, Won Hee, Peterchev, Angel V., Fröhlich, Flavio, 2015. Transcranial direct current stimulation (tDCS) of frontal cortex decreases performance on the WAIS-IV intelligence test. *Behav. Brain Res.* 290 (September), 32–44. <https://doi.org/10.1016/j.bbr.2015.04.031>.
- Sellers, Kristin K., Yu, Chunxiu, Zhou, Zhe Charles, Stitt, Iain, Li, Yuhui, Radtke-Schuller, Susanne, Alagapan, SankaraIengam, Fröhlich, Flavio, 2016. Oscillatory dynamics in the frontoparietal attention network during sustained attention in the ferret. *Cell Rep.* 16 (11), 2864–2874. <https://doi.org/10.1016/j.celrep.2016.08.055>.
- Skinner, Henri Etel, Giesbrecht, Barry, 2025. Beyond detection rate: understanding the vigilance decrement using signal detection theory. *Front. Cogn.* 3 (January), 1505046. <https://doi.org/10.3389/fcogn.2024.1505046>.
- Stitt, I., Zhou, Z.C., Radtke-Schuller, S., Fröhlich, F., 2018. Arousal dependent modulation of thalamo-cortical functional interaction. *Nature Communications* 9 (1), 2455. <https://doi.org/10.1038/s41467-018-04785-6>.
- Tucha, Lara, Fuermaier, Anselm B.M., Koerts, Janneke, Buggenthin, Rieka, Aschenbrenner, Steffen, Weisbrod, Matthias, Thome, Johannes, Lange, Klaus W., Tucha, Oliver, 2017. Sustained attention in adult ADHD: time-on-task effects of

- various measures of attention. *J. Neural Transm. (Vienna, Austria.)*: 1996; 124 (1), 39–53. <https://doi.org/10.1007/s00702-015-1426-0>.
- Webster, Donna M., Richter, Linda, Kruglanski, Arie W., 1996. On leaping to conclusions when feeling tired: mental fatigue effects on impressional primacy. *J. Exp. Soc. Psychol.* 32 (2), 181–195. <https://doi.org/10.1006/jesp.1996.0009>.
- Weissman, D.H., Roberts, K.C., Visscher, K.M., Woldorff, M.G., 2006. The neural bases of momentary lapses in attention. *Nat. Neurosci.* 9 (7), 971–978. <https://doi.org/10.1038/nn1722>.
- Yao, Linming, Wang, Yajing, Gao, Yanzhong, Gao, Hongwei, Guo, Xufeng, 2023. The role of the fronto-parietal network in modulating sustained attention under sleep deprivation: an functional magnetic resonance imaging study. *Front. Psychiatry* 14, 1289300. <https://doi.org/10.3389/fpsyg.2023.1289300>.
- Young, Jared W., Light, Gregory A., Marston, Hugh M., Sharp, Richard, Geyer, Mark A., 2009. The 5-choice continuous performance test: evidence for a translational test of vigilance for mice. *PloS One* 4 (1), e4227. <https://doi.org/10.1371/journal.pone.0004227>.
- Yu, Chunxiu, Li, Yuhui, Stitt, Iain M., Zhou, Zhe Charles, Sellers, Kristin K., Fröhlich, Flavio, 2018. Theta oscillations organize spiking activity in higher-order visual thalamus during sustained attention. *eNeuro* 5 (1), ENEURO.0384-17.2018. <https://doi.org/10.1523/ENEURO.0384-17.2018>.
- Yu, Shijing, Mückschel, Moritz, Beste, Christian, 2022. Superior frontal regions reflect the dynamics of task engagement and theta band-related control processes in time-on task effects. *Sci. Rep.* 12 (1), 846. <https://doi.org/10.1038/s41598-022-04972-y>.
- Zhou, Zhe Charles, Yu, Chunxiu, Sellers, Kristin K., Fröhlich, Flavio, 2016. Dorso-lateral frontal cortex of the ferret encodes perceptual difficulty during visual discrimination. *Sci. Rep.* 6 (March), 23568. <https://doi.org/10.1038/srep23568>.